Deliverable Report

Deliverable No: D2.1

Deliverable Title: OAM beam deviation matrix

Grant Agreement number: 255914

Project acronym: PHORBITECH

Project title: A Toolbox for Photon Orbital Angular Momentum Technology

Project website address: www.phorbitech.eu

Name, title and organisation of the scientific representative of deliverable's lead beneficiary (task leader):

Prof. Han Woerdman
Universiteit Leiden
Leiden, The Netherlands

Deliverable table

Deliverable no.	D2.1
Deliverable name	OAM beam deviation matrix
WP no.	2
Lead beneficiary no.	6 (ULEID)
Nature	R
Dissemination level	PU
Delivery date from Annex I	Month 12
Actual delivery date	3rd October 2011

D2.1) OAM beam deviation matrix: Experimental determination of the 4x4 matrix of OAM-beam angular and translational deviations from the predictions of geometrical optics, describing the "orbital Hall effect of light" and the Goos-Hänchen and Imbert-Fedorov effects, and comparison with theoretical predictions. *[Excerpt from GA-Annex I DoW]*

The present deliverable is composed of the following six publications, which are also attached in the following pages.

List of publications

[1] Quadrant detector calibration for vortex beams. N. Hermosa, A. Aiello, J.P. Woerdman, Opt.Lett. 36, 409 (2011).
[2] Demonstration of a quasi-scalar angular Goos–Hänchen effect. M. Merano, N. Hermosa, A. Aiello, J. P. Woerdman, Opt. Lett. 35, 21, 3562-3564 (2010).
[3] How orbital angular momentum affects beam shifts in optical reflection. M. Merano, N. Hermosa, J. P. Woerdman, Phys. Rev. A 82, 023817 (2010).
[4] Orbital angular momentum induced beam shifts. N. Hermosa, M. Merano, A. Aiello, J.P.Woerdman, Proc. SPIE Vol.7950, 79500F, pp1-7 (2011).
[5] Spin Hall effect of light in metallic reflection. N. Hermosa, A.M. Nugrowati, A. Aiello, J.P. Woerdman. Posted at arXiv: 1106.2009.
[6] Goos-Hänchen and Imbert-Fedorov shifts of a nondiffracting Bessel beam. A. Aiello and J.P. Woerdman, Opt. Lett. 36, 543 (2011).

Quadrant detector calibration for vortex beams

N. Hermosa,[1,*] A. Aiello,[2] and J. P. Woerdman[1]

[1]*Huygens Laboratory, Leiden University, P.O. Box 9504, 2300 RA Leiden, The Netherlands*

[2]*Max Planck Institute for the Science of Light, Günther-Scharowsky-Straße 1/Bau 34, 91058 Erlangen, Germany*

**Corresponding author: hermosa@molphys.leidenuniv.nl*

Received November 18, 2010; revised December 15, 2010; accepted December 16, 2010;
posted January 6, 2011 (Doc. ID 138408); published January 31, 2011

This Letter reports an experimental and theoretical study of the response of a quadrant detector (QD) to an incident vortex beam, specifically a Laguerre–Gaussian (LG) beam. We have found that the LG beam response depends on the vorticity index ℓ. We compare LG beams with hard-ringed beams and find that at higher ℓ values, the QD response to LG beams can be approximated by its response to hard-ringed beams. Our findings are important in view of the increasing interest in optical vortex beams.

OCIS codes: 040.5160, 120.4640.

Great attention has been given to optical vortex beams such as the Laguerre–Gaussian (LG) donut beams [1]. This is reflected by the range of research from diverse fields such as optical tweezing and micromanipulation [2,3], second-harmonic generation [4], spontaneous and stimulated parametric downconversion [5,6], microscopy [7], quantum communication [8], plasma physics [9], and even in antennas designed for advanced gravitational waves detection [10]. This broad spectrum of applications makes it useful to develop methods for accurate determination of the spatial position of such beams.

A direct method of position measurement of beams in general, is by means of a quadrant detector (QD). The QD is a position sensitive device which is composed of four identical $p-n$ junction photodiodes separated by very small gaps. Being part of the family of position-sensitive devices that includes the lateral effect photodiodes [11], the QD has an advantage of higher resolution and lower inherent noise, making it more useful for micro/nanometer displacement measurement compared to lateral effect photodiodes [12].

There is currently an interest in the response characteristics of quadrant detectors in general. Cui *et al.* increased the QD's measurement accuracy by improving its linearity index [12], while two other groups have focused on other characteristics, one on the detection sensitivity of these detectors with respect to optical beam sizes [13], and the other on the influence of the intensity of the incident beam [14]. However, all investigations have focused so far on the fundamental Gaussian beams.

Recently, we have used a QD in experiments on reflective beam shifts of Gaussian vortex beams [15]. This requires a proper understanding of the response of the QD to such beams. The purpose of our letter is to present this understanding in detail. Specifically, we look at the response of the QD to Gaussian optical vortices (i.e., LG donut beams) with different values of ℓ. We also compare these results to the responses when "hard-ringed" beams are used, as opposed to the "soft-ringed" LG donut beams. We defined a "hard-ringed" beam as having step-like edges compared to the "soft-ringed" beam with a Gaussian dependence of the intensity profile. In the succeeding paragraphs, we present theoretical calculations and experimental results.

We determine the response of the quadrant detector to ring-type beams by defining its dimensionless response in both the X and Y directions. These responses are given by the expressions

$$\frac{I_x}{I}=\frac{I_A+I_C-(I_B+I_D)}{I_A+I_B+I_C+I_D},\qquad \frac{I_y}{I}=\frac{I_A+I_B-(I_C+I_D)}{I_A+I_B+I_C+I_D},\tag{1}$$

where I_A, I_B, I_C, and I_D are the photocurrents detected by the photodiode panels A, B, C, and D of the quadrant detector as shown in Fig. 1; $I_i \propto \int\int I(x,y)\mathrm{d}x\mathrm{d}y$, where $i=A, B, C$, and D are the panels of the QD, and $I(x,y)$ is the intensity distribution at the QD. First, we restrict ourselves to $\mathrm{LG}_{\ell,p}$ beams with $p=0$ (i.e., one-ring donut beams) whose intensity distribution is given by

$$I(x,y)=\frac{2}{\pi\omega_z^2}\frac{1}{|\ell|!}\left[\frac{2}{\omega_z^2}(x^2+y^2)\right]^{|\ell|}e^{-\frac{2}{\omega_z^2}(x^2+y^2)},\tag{2}$$

where ω_0 is the waist of the fundamental Gaussian beam, z is the axis of propagation, $\omega_Z=\omega_0\sqrt{1+\frac{z^2}{L^2}}$ is the beam radius at position z, and $L=\frac{k\omega_0^2}{2}$ is the Rayleigh length. The dimensionless response $\frac{I_X}{I}$ that is given by

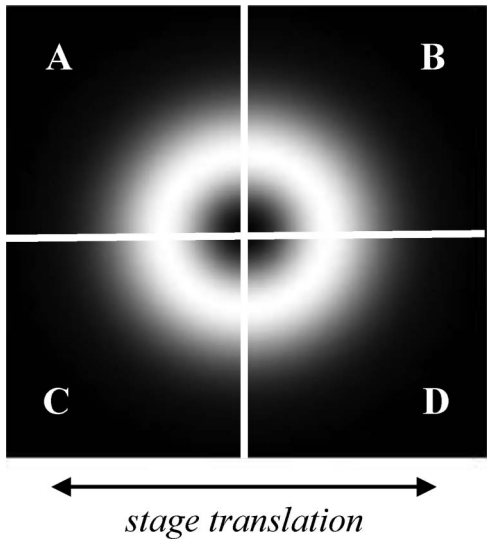

Fig. 1. LG beam incident on a quadrant detector. The difference in the photocurrents from the four panels is related to the displacement of the beam from the center.

Table 1. Calibration Constants K for the Dimensionless Response ($\frac{I_x}{I} = K\Delta x$) of the Quadrant Detector with Different Beam Profiles at Displacement Δx Much Smaller Than the Diameter of the Beam

Beam Profile	Calibration Constant K
Laguerre–Gaussian beam	$\frac{2^{3/2}\Gamma(\frac{1}{2}+\lvert\ell\rvert)}{\omega_z\pi\lvert\ell\rvert!}$
Hard-ringed beam of outer radius R_1 and inner radius R_2	$\frac{4}{\pi R_1(1+\frac{R_2}{R_1})}$
Top-hat beam of radius R	$\frac{4}{\pi R}$

$$\frac{I_x}{I} = \frac{\int_0^x \int_0^\infty I(x,y)\mathrm{d}y\mathrm{d}x}{\int_0^\infty \int_0^\infty I(x,y)\mathrm{d}y\mathrm{d}x} \tag{3}$$

reduces, when using Eq. (2), to

$$\frac{I_x}{I} = \frac{2^{3/2}\Gamma\left(\frac{1}{2}+|\ell|\right)x}{\omega_z\pi|\ell|!} \tag{4}$$

when the displacement x is much less than the width of the beam.

Table 1 summarizes the different theoretical responses of the QD in the limit of small beam displacements. We give results for LG beams (as discussed above), for hard-ringed beams and for a top-hat beam. It is interesting to compare these cases, although of course only the LG beams are vortex beams.

In our experiment, we used a commercial quadrant detector (New Focus, model 2901) mounted to a linear translator (Newport LTA-HL) controlled by a computer. The overall size of the QD is 3 mm × 3 mm while the separation channel between the photodiodes is 100 μm wide. The QD was connected to a nanovoltmeter that measured the minute voltage differences as the QD was translated in its own plane (<150 μm). A He–Ne laser (632.8 nm) was used as the light source and was carefully aligned such that it impinged orthogonal to the QD. The LG beams ($LG_{\ell 0}$) were produced with a cylindrical lens mode-converter from a He–Ne laser that was forced to oscillate with higher-order Hermite Gaussian beams (HG_{n0}), as described in [16]. The beam waist ω_0 of the fundamental Gaussian beam was measured to be 620 μm.

The hard-ringed and top-hat beams were produced as follows. The waists of the fundamental Gaussian laser beam was expanded up to 20 times (i.e., up to 12 mm) and was apertured to an outer radius R_1 of 1.2 mm for the top-hat beam and additionally to an inner radius R_2 of 0.300 mm, 0.600 mm, and 0.900 mm to produce the hard-ringed beams. These apertures were placed very close to the QD to reduce diffraction effects.

Figure 2 shows the theoretical prediction (curve) based on Table 1 for an LG beam with beam waist of 620 μm and $z = 0$, as one goes from $\ell = 0$ to higher ℓ values. There is a good agreement with our experimental data (squares). Note that the experiment is restricted to integer values of ℓ; the theoretical curve is continuous since $\Gamma(|\ell|)$ and $|\ell|!$ are defined for all values of $|\ell|$. The K values displayed in Fig. 2 are the slopes of the dimensionless response (I_x/I) as a function of the translation Δx of the QD perpendicularly to the incident beam while still

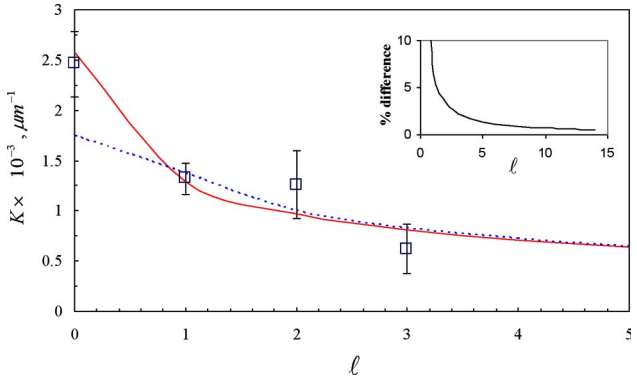

Fig. 2. (Color online) Calibration constant K_{LG} varies for different values of ℓ. Larger ℓ values give smaller calibration constants. The drawn curve is the theoretical prediction, while the points marked by open squares are experimentally obtained, both for LG beams. The error bars are mainly attributed to the imperfect purity of the LG mode. The dashed curve shows the theoretical prediction when the LG soft-ring beam is approximated as a hard ring (see text). The hard-ring beam at $\ell = 0$ is a top-hat beam. The inset is the percent difference between the solid curve and the dashed curve.

remaining in the linear region of the response of the QD. The calibration constant for LG beams K_{LG} decreases asymptotically as ℓ values are increased. The change of the value of K_{LG} is drastic, with a drop of 50% from $\ell = 0$ to $\ell = 1$. By $\ell = 10$, the value of K_{LG} has dropped to ~17% of its value at $\ell = 0$.

It is interesting to compare the QD response on LG beams to that of hard-ringed beams. In this context, we choose the thickness of the equivalent hard-ringed beam as the FWHM of the soft ring of the LG beam. We approximate the outer radius R_1 of the hard ring with the sum of the radius of the LG mode ($R_{\max I} = \omega\sqrt{\frac{\ell}{2}}$) and half of the FWHM thickness of the LG ring. For the inner radius R_2, we subtract half of the FWHM ring thickness from the LG ring radius. The dashed curve in Fig. 2 gives the theoretical calibration constant for an LG beam when we use the hard-ring approximation as discussed above. The inset shows a decreasing difference in the K values as ℓ increases. The difference between the K_{LG} and

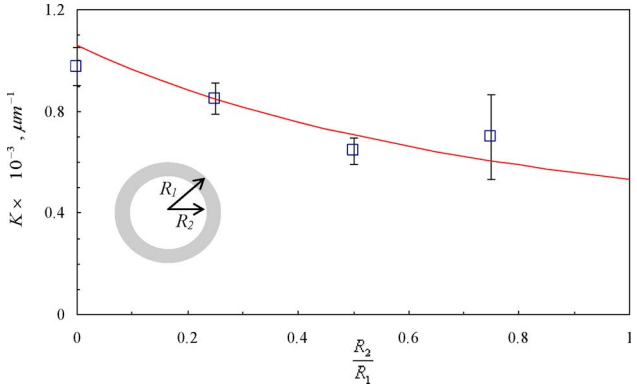

Fig. 3. (Color online) Calibration constant K of a hard-ring beam as a function of (R_2/R_2). Solid curve, the theoretical prediction while the points marked by open squares are experimentally obtained. We ascribed the error bars to the noise implied by the low intensity of the hard-ring beams.

$K_{\text{Hard ring}}$ at $\ell = 1$ is 6.5%, while at $\ell = 10$ this becomes as small as ~0.7%. However the value of K_{LG} at $\ell = 0$ differs largely from its approximation as a top-hat beam.

Figure 3 shows the response of the QD for hard-ringed beams as a function of the ratio (R_2/R_1). A top-hat beam corresponds to $R_2 = 0$. Our experimental results agree with the theoretical prediction that is calculated based on the experimental parameters: $R_1 = 1.2$ mm and $R_2 =$ 0.300 mm, 0.600 mm, and 0.900 mm. As the ratio of the radii becomes larger, the value of $K_{\text{Hard ring}}$ becomes smaller.

In conclusion, we have reported the response of a quadrant detector to LG beams. The accurate measurement of positional displacement of an LG beam is important in view of the growing interest in vortex beams. We see both in theory and experiments that the calibration constant K_{LG} depends on the topological charge, ℓ. With higher ℓ values, the LGs can be considered as hard-ringed beams when exciting a QD. Such high-ℓ vortex beams are important for optical tweezing and trapping, see [17], and possibly for gravitational-wave detection [18].

Our work is part of the Foundation for Fundamental Research of Matter (FOM). It is also supported by the European Union (EU) within FET Open-FP7 ICT as part of the STREP Program 255914 PHORBITECH. A. Aiello acknowledges support from the Alexander von Humboldt Foundation.

References

1. L. Allen, M. W. Beijersbergen, R. J. C. Spreeuw, and J. P. Woerdman, Phys. Rev. A **45**, 8185 (1992).
2. D. Grier, Nature **424**, 810 (2003).
3. A. Picón, A. Benseny, J. Mompart, J. R. Vázquez de Aldana, L. Plaja, G. F. Calvo, and L. Roso, New J. Phys. **12**, 083053 (2010).
4. J. Courtial, K. Dholakia, L. Allen, and M. J. Padgett, Phys. Rev. A **56**, 4193 (1997).
5. A. Mair, A. Vaziri, G. Weihs, and A. Zeilinger, Nature **412**, 313 (2001).
6. D. P. Caetano, M. P. Almeida, P. H. Souto Ribeiro, J. A. O. Huguenin, B. Coutinho dos Santos, and A. Z. Khoury, Phys. Rev. A **66**, 041801 (2002).
7. T. Watanabe, Y. Iketaki, T. Omatsu, K. Yamamoto, M. Sakai, and M. Fujii, Opt. Express **11**, 3271 (2003).
8. G. Molina-Terriza, J. P. Torres, and L. Torner, Nature Phys. **3**, 305 (2007).
9. J. Hamazaki, R. Morita, K. Chujo, Y. Kobayashi, S. Tanda, and T. Omatsu, Opt. Express **18**, 2144 (2010).
10. J.-Y. Vinet, Phys. Rev. D **82**, 042003 (2010).
11. H. J. Woltring, IEEE Trans. Electron. Devices **22**, 581 (1975).
12. S. Cui and Y. C. Soh, Appl. Phys. Lett. **96**, 081102 (2010).
13. E. J. Lee, Y. Park, C. S. Kim, and T. Kouh, Curr. Appl. Phys. **10**, 834 (2010).
14. Y. Panduputra, T. W. Ng, A. Neild, and M. Robinson, Appl. Opt. **49**, 3669 (2010).
15. M. Merano, N. Hermosa, A. Aiello, and J. P. Woerdman, Phys. Rev. A **82**, 023817 (2010).
16. M. W. Beijersbergen, L. Allen, H. E. L. O. van der Veen, and J. P. Woerdman, Opt. Commun. **96**, 123 (1993).
17. S. Sundbeck, I. Gruzberg, and D. Grier, Opt. Lett. **30**, 477 (2005).
18. M. Granata, C. Buy, R. Ward, and M. Barsuglia, Phys. Rev. Lett. **105**, 231102 (2010).

Demonstration of a quasi-scalar angular Goos–Hänchen effect

M. Merano,[1,*] N. Hermosa,[1] A. Aiello,[2] and J. P. Woerdman[1]

[1]*Huygens Laboratory, Leiden University, P.O. Box 9504, 2300 RA Leiden, The Netherlands*

[2]*Max Planck Institute for the Science of Light, Günter-Scharowsky-Strasse 1/Bau 24, 91058 Erlangen, Germany*

**Corresponding author: merano@molphys.leidenuniv.nl*

Received July 8, 2010; accepted August 9, 2010;
posted September 29, 2010 (Doc. ID 131289); published October 19, 2010

We show experimentally that the angular Goos–Hänchen (GH) effect can be easily observed, also without employing its resonant enhancement at Brewster incidence. An *s*-polarized beam was used to decouple the polarization from the propagation dynamics of the beam. We found that, in this case, the angular GH effect can be strongly enhanced by increasing the angular aperture of the Gaussian beam. Our experiments suggest a route toward observing the angular GH effect for true scalar waves, such as acoustic waves and quantum matter waves.

OCIS codes: 240.3695, 260.5430.

The Goos–Hänchen (GH) effect is the longitudinal displacement, with respect to the predictions of geometrical optics, of a light beam totally reflected by a planar interface [1]. As one of the corrections to the law of reflection when a bounded beam is considered instead of plane waves, the GH shift has been extensively investigated, both for its fundamental interest and for its relevance in optical metrology. The GH shift, typically of the order of a wavelength, was first observed in the case of a light beam undergoing a series of total internal reflections (TIRs) at a glass–air interface [1]. In recent years, much progress has been made in the observation of the GH effect using different techniques (see papers cited in [2,3]), including investigations of the effect in single reflection [2,4].

The corrections to geometrical reflection for a light beam incident at an interface between two media are not limited to positional shifts alone. We have recently reported the first experimental observation of a new effect in optics [3], an *angular* deviation of the beam axis with respect to ray optics predictions (Fig. 1). A similar angular deviation was recently observed in the microwave domain [5]. This was theoretically proposed in the 1970s [6,7] and, since then, has been the subject of a number of theoretical investigations [8–10]. Its name, angular GH shift (Θ_{AGH}), comes from the fact that the angular displacement of the beam axis takes place in the plane of incidence. This angular effect appears only in a non-TIR configuration (e.g., in external reflection) in contrast to the positional GH shift that occurs only in TIR [3]. Both effects belong to a whole category of perturbative corrections to geometrical optics [10–14]. In our previous work [3], we greatly magnified the angular effect by exploiting the Brewster resonance. This resonance is a direct consequence of the vector nature of light, which appears when the light field vector oscillates in the plane of incidence (*p* polarization). It is, therefore, relevant to ask: *Can the angular GH effect be observed for scalar waves or is it practically restricted to vector waves?*

It is well known that the *positional* GH shift *can* be observed for scalar waves. For example, the displacement of an acoustic wave beam, reflected at a liquid–solid interface [15] has been reported [16]. In acoustics, the positional GH shift is most prominent at or near the Rayleigh angle, where a leaky surface wave is generated by the incident beam [17]. In analogy with optics, positional GH shifts of acoustic beams are also observed on more complex structures, such as periodically corrugated interfaces; this also allows the positional GH to become negative [18,19].

Another scalar variety of the positional GH effect occurs for particles; propagation of particles in quantum mechanics is described by wave functions (matter waves). It was predicted that an electron beam, totally reflected at a potential barrier, experiences a positional GH [20]. This effect is expected also in atom optics where ultracold atoms are manipulated by laser fields [21]. Recently, the observation of the positional GH with neutrons was reported as a first experimental evidence of this effect in matter waves [22]. We note that the equation for the GH shift of a neutron beam is the same as that for the GH shift of an *s*-polarized light beam [23,24]. This allows us to realize a quasi-scalar implementation of the angular GH effect.

Our experimental setup is shown in Fig. 2. A Gaussian light beam is obliquely incident on a BK7 prism ($n = 1.51$). A superluminescent single-mode-fiber-pigtailed diode (SLED) that provides 2 mW of cw radiation at $\lambda = 820$ nm is used as the light source. The beam that leaves the exit facet of the SLED fiber is collimated by a microscope objective. The $1/e^2$ intensity radius w_0 of the collimated beam after the microscope objective is 1.62 mm. The beam is then *s* polarized by means of a Glan polarizing prism. A cylindrical lens ($f = 7.5$ cm)

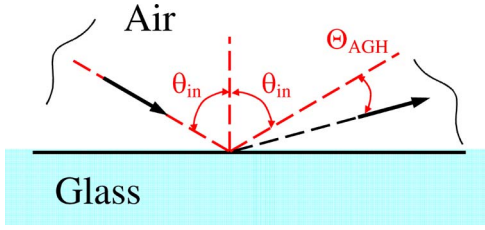

Fig. 1. (Color online) A TEM_{00} Gaussian beam hits an air–glass interface. The reflected beam suffers the angular Goos–Hänchen effect. The angular deviation of the axis of the reflected beam relative to the specular direction is labeled as Θ_{AGH}.

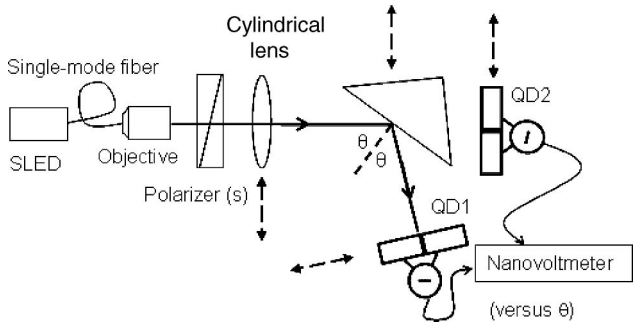

Fig. 2. Setup to measure nonspecular reflection over a wide range of incident angles and with different beam angular apertures θ_0. Reflection takes place at the surface of a right-angle BK7 glass prism. We measure the angular shift for a light beam focused by a cylindrical lens. See the text for details of the experimental procedure.

is used to avoid cross polarization [25,26], which would otherwise spoil the pure s polarization. The cylindrical lens produces a sheet beam that is focused in one plane to $w_0 = 12\ \mu$m ($\theta_0 = 22$ mrad); this focus is located 1 cm in front of the air–prism interface. We exploit the fact that, theoretically, Θ_{AGH} scales with θ_0^2, where $\theta_0(\theta_0 = \lambda/\pi w_0)$ is the beam angular aperture and w_0 is the beam waist (see below) [3,9]. We use a quadrant detector (QD1) to measure the angular deviation of the reflected beam with respect to reflection of a collimated beam. The QD1 signal is fed into a nanovoltmeter in order to detect the beam displacement. The distance in between the QD1 and the prism reflecting surface is 5 cm. The lens, the quadrant detectors, and the prism are mounted on linear translation stages, while the prism is mounted on a rotation stage.

The beam is carefully aligned by first removing the prism and the focusing lens. The collimated beam at the exit of the polarizer is sent to a second quadrant detector (QD2). With the help of a translation stage, the beam is centered on QD2 by reading a null signal on the nanovolmeter. A focusing lens is inserted exactly on the beam axis, making sure that the beam is still perfectly centered on QD2. The prism is then introduced in the setup, while the reflected beam is centered exactly on QD1. The final step consists of removing the focusing lens and recording the displacement of the beam with respect to its position with the focusing lens. This can be done in two ways: (1) by reading the nanovolmeter and calculating the displacement using a calibration curve, and/or (2) by linearly translating the stage of QD1 and recording the distance traversed by the translation stage until a null signal is read.

Figure 3 shows the theoretical prediction (line) of Θ_{AGH} as a function of the angle of incidence. The equation giving $\Theta_{\mathrm{AGH}}(\theta)$ as a function of the angle of incidence for an s-polarized beam is [3,6,9]

$$\Theta_{\mathrm{AGH}}(\theta) = \theta_0^2 \frac{\sin\theta}{\sqrt{n^2 - \sin^2\theta}}. \qquad (1)$$

There is good agreement with the experimental data (circles). In our experiment, the value of Θ_{AGH} is of the order of a few 100 μrad, i.e., 4 orders of magnitude enhanced

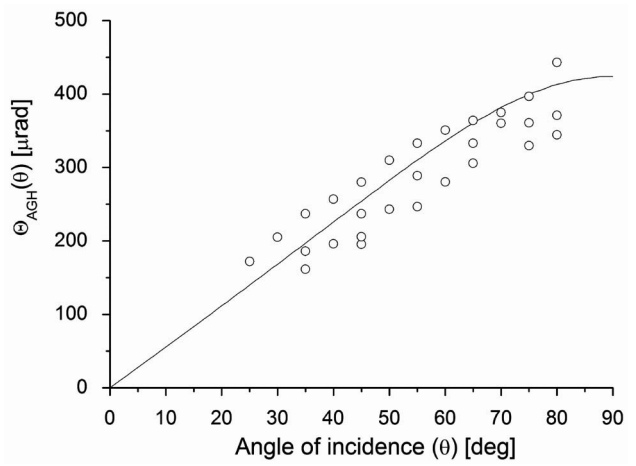

Fig. 3. The theoretical curve gives the angular shift versus the angle of incidence for an s-polarized light beam with a wavelength of 820 nm, focused to a spot size of 12 μm. Dots are experimental data.

relative to the value expected for a "standard" laser beam with a width of, say, 1 mm. In fact, Fig. 3 displays the angular shift for the focused beam with respect to the collimated beam. The 1 mm width laser beam is used as a reference for perfect ("geometrical") reflection, because its angular deviation is negligible, being very much smaller than our experimental error of 50 μrad.

Although the nominal spot size w_0 expected as a consequence of focusing by an ideal cylinder lens is 12 μm, the measured value is larger, namely, 17 μm. This is due to the aberrations introduced by the cylindrical lens, a simple plano-convex lens. We observe anyway that Θ_{AGH} is not affected by aberrations (the theoretical shift for a Gaussian beam focused by an ideal cylinder lens to a $w_0 = 17\ \mu$m is a factor of 2 smaller that what we observe). Indeed, geometrical-optics aberrations *do* affect the focal spot size but *do not* affect the wave-vector spreading of our beam. For instance, spherical aberration simply corresponds to an NA-dependent *axial* displacement of the ideal focus.

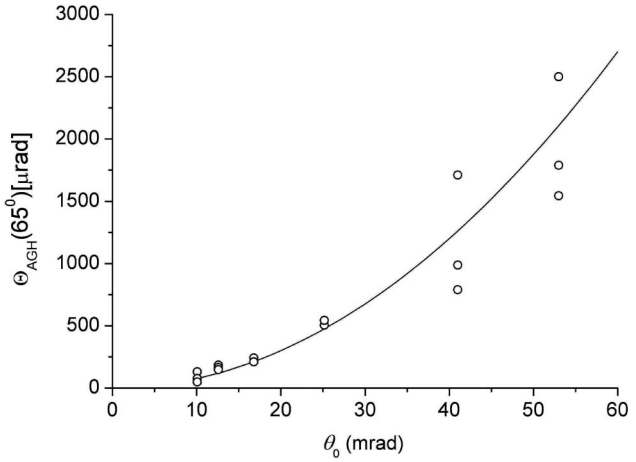

Fig. 4. The angular GH shift increases with the square of the beam's angular aperture. The solid curve corresponds to the theoretical prediction from Eq. (1). The angular aperture was changed by using cylindrical lenses of different focal lengths.

Finally, we verified the relationship of Θ_{AGH} and the beam's angular aperture θ_0. This aperture can be varied by using cylindrical lenses of different focal lengths while keeping the angle of incidence on the prism constant at 65°. Figure 4 shows that our experimental results agree well with the theoretical prediction given by the solid curve: Θ_{AGH} increases with the square of the beam's angular aperture. By tightly focusing the beam, Θ_{AGH} can be enhanced.

In conclusion, we have reported the experimental observation of Θ_{AGH} for a quasi-scalar wave beam. The polarization of the incident light beam (*s*-polarized beam) is orthogonal to the plane of incidence and does not play a role in the angular deviation of the beam. We have found that the key to easy observation of Θ_{AGH} is by enhancing the effect with a relatively large angular aperture of the beam θ_0; this should hold equally for true scalar beams, such as acoustic and matter beams.

This work is part of the program of the foundation for "Fundamenteel Onderzoek der Materie"; it is also supported by the European Commission as part of the FET-Open program 255914 ("PHORBITECH"). A. A. acknowledges support from the Alexander von Humboldt Foundation.

References and Notes

1. F. Goos and H. Hänchen, Ann. Phys. **436**, 333 (1947).
2. F. Bretenaker, A. L. Floch, and L. Dutriaux, Phys. Rev. Lett. **68**, 931 (1992).
3. M. Merano, A. Aiello, M. P. van Exter, and J. P. Woerdman, Nat. Photon. **3**, 337 (2009).
4. M. Merano, A. Aiello, G. W. 't Hooft, M. P. van Exter, E. R. Eliel, and J. P. Woerdman, Opt. Express **15**, 15928 (2007).
5. D. Müller, D. Tharanga, A. A. Stahlhofen, and G. Nimtz, Europhys. Lett. **73**, 526 (2006).
6. J. W. Ra, H. L. Bertoni, and L. B. Felsen, SIAM J. Appl. Math. **24**, 396 (1973).
7. Y. M. Antar and W. M. Boerner, Can. J. Phys. **52**, 962 (1974).
8. C. C. Chan and T. Tamir, Opt. Lett. **10**, 378 (1985).
9. M. A. Porras, Opt. Commun. **131**, 13 (1996).
10. W. Nasalski, J. Opt. Soc. Am. A **13**, 172 (1996).
11. A. Aiello and J. P. Woerdman, Opt. Lett. **33**, 1437 (2008).
12. K. Y. Bliokh and Y. P. Bliokh, Phys. Rev. Lett. **96**, 073903 (2006).
13. V. G. Fedoseyev, Opt. Commun. **282**, 1247 (2009).
14. O. Hosten and P. Kwiat, Science **319**, 787 (2008).
15. Acoustic waves are not scalar waves in general. For example, acoustic waves in solid-state physics can be nonscalar.
16. A. Schoch, Acustica **2**, 18 (1952).
17. H. L. Bertoni and T. Tamir, Appl. Phys. **2**, 157 (1973).
18. C. Bonnet, D. Chauvat, O. Emile, F. Bretenaker, A. L. Floch, and L. Dutriaux, Opt. Lett. **26**, 666 (2001).
19. A. Teklu, M. A. Breazeale, N. F. Declercq, R. D. Hasse, and M. S. McPherson, J. Appl. Phys. **97**, 084904 (2005).
20. S. C. Miller, Jr., and N. Ashby, Phys. Rev. Lett. **29**, 740 (1972).
21. J. Huang, Z. Duan, H. Y. Ling, and W. Zhang, Phys. Rev. A **77**, 063608 (2008).
22. V. O. de Haan, J. Plomp, T. M. Rekveldt, W. H. Kraan, and A. A. van Well, Phys. Rev. Lett. **104**, 010401 (2010).
23. M. Maaza and B. Pardo, Opt. Commun. **142**, 84 (1997).
24. The difference between a neutron and a photon from a spin (polarization) point of view is as follows. A neutron is a massive particle whose spin ½ is not coupled to the propagation direction of the neutron beam; contrarily, a photon is a zero-mass particle whose paraxial spin ½ is either parallel or antiparallel with the propagation direction of the photon beam.
25. Y. Fainman and J. Shamir, Appl. Opt. **23**, 3188 (1984).
26. A. Aiello, M. Merano, and J. P. Woerdman, Opt. Lett. **34**, 1207 (2009).

How orbital angular momentum affects beam shifts in optical reflection

M. Merano, N. Hermosa, and J. P. Woerdman
Huygens Laboratory, Leiden University, P.O. Box 9504, NL-2300 RA Leiden, The Netherlands

A. Aiello
Max Planck Institute for the Science of Light, Günter-Scharowsky-Straße 1/Bau 24, D-91058 Erlangen, Germany

(Received 3 March 2010; published 24 August 2010)

It is well known that reflection of a Gaussian light beam (TEM_{00}) by a planar dielectric interface leads to four beam shifts when compared to the geometrical-optics prediction. These are the spatial Goos-Hänchen (GH) shift, the angular GH shift, the spatial Imbert-Fedorov (IF) shift, and the angular IF shift. We report here, theoretically and experimentally, that endowing the beam with orbital angular momentum leads to coupling of these four shifts; this is described by a 4×4 mixing matrix.

DOI: 10.1103/PhysRevA.82.023817 PACS number(s): 42.79.−e, 41.20.Jb, 42.25.Gy, 78.20.−e

I. INTRODUCTION

The reflection of a light beam by a mirror shows subtle aspects that were first conjectured by Newton [1]: The center of the reflected beam may show a small spatial shift *in* the plane of incidence relative to the position predicted by geometrical optics. This shift has been named after Goos and Hänchen (GH), who were the first to observe it in total internal reflection (TIR) [2]. Additionally, there is a spatial shift *perpendicular* to the plane of incidence, the so-called Imbert-Fedorov shift (IF) [3,4]. There exist also *angular* GH and IF shifts, both of which have been demonstrated recently in external reflection [5,6]. The angular shifts can be seen as shifts in wave-vector space [6–8]. All these shifts depend on the polarization of the incident photons. Accurate calculations of either GH or IF shifts (or both) can be found in Refs. [9–11]. In more recent years the GH shift has been studied in a large diversity of cases, ranging from photonic crystals [12] to neutron optics [13].

We are interested in the question of how these beam shifts are affected when the light beam is endowed with orbital angular momentum (OAM). OAM is a relatively novel degree of freedom of a light beam that can be found in applications from optical tweezers to quantum information science [14,15]. Theoretically, a treatment of the effect of OAM on beam shifts has already been given, first by Fedoseyev [16–18] and then by Bliokh *et al.* [19]. Here we prefer to develop our own theoretical treatment based on straightforward application of Snell's law and the Fresnel equations, in order to derive a unified matrix formalism for the four basic shifts: spatial GH, angular GH, spatial IF, and angular IF. Experimentally, Okuda and Sasada have studied the deformation of an OAM carrying beam using TIR very close to the critical angle [20]; however, they did not report GH and IF shifts. Dasgupta and Gupta have measured the IF shift of an OAM beam reflected by a dielectric interface, but only for the spatial case [21].

It is the purpose of this article to report a theoretical and experimental study of the effect of OAM on the four basic shifts: spatial GH, angular GH, spatial IF, and angular IF. We find that these shifts are coupled by OAM; this is described by an OAM-dependent 4×4 mixing matrix. We have experimentally confirmed this mixed occurrence of GH and IF shifts.

II. THEORY

In this section we furnish a thorough theoretical analysis for the problem of the reflection of an OAM-carrying light beam by a dielectric interface.

Consider a monochromatic beam containing a continuous distribution of wave vectors $\mathbf{k}$ centered around $\mathbf{k}_0 = k_0 \hat{\mathbf{z}}_i$, where $\hat{\mathbf{z}}_i$ is a unit vector along the central propagation direction of the incident beam: $\mathbf{k} = k_0 \hat{\mathbf{k}} = \mathbf{k}_0 + \mathbf{q}$, with $\mathbf{q} = \mathbf{q}_T + q_L \hat{\mathbf{z}}_i$ and $\mathbf{q}_T \cdot \hat{\mathbf{z}}_i = 0$. Using the notation of Fig. 1, we write $q_T/k_0 = \sin\alpha$ and $q_L/k_0 = 1 - \cos\alpha$ with $q_T = |\mathbf{q}_T|$ and $\alpha = \arccos(\hat{\mathbf{k}} \cdot \hat{\mathbf{k}}_0)$. A collimated beam has a narrow distribution of wave vectors around $\mathbf{k}_0$ such that $\sin\alpha \cong \alpha \ll 1$ with $q_T/k_0 \cong \alpha \ll 1$ and $q_L/k_0 \cong (q_T/k_0)^2/2$. Thus, if we write $\mathbf{k} = k_0(\hat{\mathbf{x}}_i U + \hat{\mathbf{y}} V + \hat{\mathbf{z}}_i W)$ with $W = \sqrt{1 - U^2 - V^2}$, we can assume $U, V \ll 1$ without significant error. Let $\mathbf{E}^I(\mathbf{r},t)$ be the electric field of the incident beam. Upon reflection, this field evolves to $\mathbf{E}^R(\mathbf{r},t)$, which is to be found. From the linearity of the wave equation it follows that $\mathbf{E}^R(\mathbf{r},t)$ can be determined by studying the action of the interface upon each plane-wave field,

$$\boldsymbol{A}^I(\mathbf{k}) = \boldsymbol{f}_\perp(\mathbf{k}) \exp(i\mathbf{k} \cdot \mathbf{r} - i\omega t), \tag{1}$$

that constitutes $\mathbf{E}^I(\mathbf{r},t)$, with $\omega = |\mathbf{k}|c$. According to Refs. [22,23], we assume the polarization-dependent amplitude of $\boldsymbol{A}^I(\mathbf{k})$ equal to $\boldsymbol{f}_\perp(\mathbf{k}) = \hat{\boldsymbol{f}} - \hat{\mathbf{k}}(\hat{\mathbf{k}} \cdot \hat{\boldsymbol{f}}) = a_p(\mathbf{k})\, \hat{\boldsymbol{x}}_\mathbf{k} + a_s(\mathbf{k})\, \hat{\boldsymbol{y}}_\mathbf{k}$, with

$$a_p(\mathbf{k}) = f_p + V f_s \cot\theta, \quad a_s(\mathbf{k}) = f_s - V f_p \cot\theta, \tag{2}$$

up to first order in U, V and $\theta = \arccos(\hat{\mathbf{z}}_i \cdot \hat{\mathbf{z}})$. Here $\hat{\boldsymbol{f}} = f_p \hat{\boldsymbol{x}}_i + f_s \hat{\mathbf{y}}$ is a unit complex vector that fixes the polarization of the incident beam, and $\hat{\mathbf{y}}_\mathbf{v} = \hat{\mathbf{z}} \times \mathbf{v}/|\hat{\mathbf{z}} \times \mathbf{v}|$ and $\hat{\boldsymbol{x}}_\mathbf{v} = \hat{\mathbf{y}}_\mathbf{v} \times \mathbf{v}$ denote a pair of mutually orthogonal real unit vectors that together with the arbitrary vector $\hat{\mathbf{v}} = \mathbf{v}/|\mathbf{v}|$ form a right-handed Cartesian reference frame $K_\mathbf{v} = \{\hat{\boldsymbol{x}}_\mathbf{v}, \hat{\mathbf{y}}_\mathbf{v}, \hat{\mathbf{v}}\}$ attached to $\mathbf{v}$.

When the beam is reflected at the interface, each plane wave evolves as $\boldsymbol{A}^I(\mathbf{k}) \to \boldsymbol{A}^R(\mathbf{k})$, where

$$\boldsymbol{A}^R(\mathbf{k}) = [r_p(\theta_\mathbf{k}) a_p \hat{\boldsymbol{x}}_{\tilde{\mathbf{k}}} + r_s(\theta_\mathbf{k}) a_s \hat{\mathbf{y}}_{\tilde{\mathbf{k}}}] \chi(\tilde{\mathbf{r}}, t) \tag{3}$$

and $\chi(\tilde{\mathbf{r}},t) = \exp(i\tilde{\mathbf{k}} \cdot \mathbf{r} - i\omega t) = \exp(i\mathbf{k} \cdot \tilde{\mathbf{r}} - i\omega t)$. The notation $\tilde{\mathbf{v}}$ indicates the mirror image of the vector $\mathbf{v}$ with

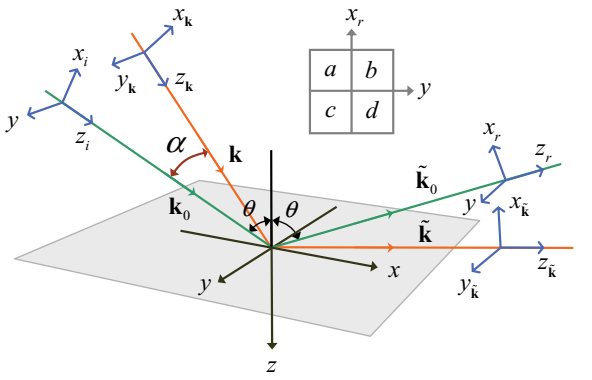

FIG. 1. (Color online) Geometry of beam reflection at a dielectric interface. The reflected wave vector $\tilde{\mathbf{k}}$ is the mirror image of the incident wave vector $\mathbf{k}$. (Inset) Quadrant detector with sensitive areas a, b, c, and d.

respect to the interface: $\tilde{\mathbf{v}} = \mathbf{v} - 2\hat{\mathbf{z}}(\hat{\mathbf{z}}\cdot\mathbf{v})$, with $\tilde{\mathbf{v}}\cdot\mathbf{u} = \mathbf{v}\cdot\tilde{\mathbf{u}}$ [24]. Moreover, $r_p(\theta_\mathbf{k})$ and $r_s(\theta_\mathbf{k})$ are the Fresnel reflection coefficients at incidence angle $\theta_\mathbf{k} = \arccos(\hat{\mathbf{k}}\cdot\hat{\mathbf{z}})$ for p and s waves, respectively. By direct calculation it is not difficult to show that, up to first order in U,V,

$$\hat{\mathbf{x}}_{\tilde{\mathbf{k}}} = \hat{\mathbf{x}}_r - V(\cot\theta)\hat{\mathbf{y}} + U\hat{\mathbf{z}}_r, \tag{4}$$

$$\hat{\mathbf{y}}_{\tilde{\mathbf{k}}} = V(\cot\theta)\hat{\mathbf{x}}_r + \hat{\mathbf{y}} - V\hat{\mathbf{z}}_r, \tag{5}$$

$$r_\lambda(\theta_\mathbf{k}) = r_\lambda + Ur'_\lambda, \tag{6}$$

where $\lambda \in \{p,s\}$, $r_\lambda = r_\lambda(\theta)$, and $r'_\lambda = \partial r_\lambda(\theta)/\partial\theta$. With the use of Eqs. (2) and (4)–(6) in Eq. (3), we obtain

$$\boldsymbol{A}^R(\mathbf{k}) = \hat{\mathbf{x}}_r A_p^R(\mathbf{k}) + \hat{\mathbf{y}} A_s^R(\mathbf{k}) + \hat{\mathbf{z}}_r A_L^R(\mathbf{k}), \tag{7}$$

where, up to first order in U,V,

$$A_\lambda^R(\mathbf{k}) = f_\lambda r_\lambda(1 + iX_\lambda U - iY_\lambda V)\chi(\tilde{\mathbf{r}},t), \tag{8}$$

$$A_L^R(\mathbf{k}) = (f_p r_p U - f_s r_s V)\chi(\tilde{\mathbf{r}},t). \tag{9}$$

Here we have defined

$$X_p = -i\frac{\partial \ln r_p}{\partial\theta}, \quad Y_p = i\frac{f_s}{f_p}\left(1 + \frac{r_s}{r_p}\right)\cot\theta, \tag{10}$$

with $X_s = X_p|_{p\leftrightarrow s}$ and $Y_s = -Y_p|_{p\leftrightarrow s}$. The limit of specular reflection is achieved by letting $r_p \to 1$ and $r_s \to -1$, where Eq. (10) reduces to $X_p = 0 = X_s$ and $Y_p = 0 = Y_s$. Notice that from Eqs. (8) and (9) it follows that for a paraxial beam the longitudinal electric-field energy density $|A_L^R|^2$ scales as $\sim\alpha^2$ and it is therefore negligible with respect to the transverse electric-field energy density $|A_p^R|^2 + |A_s^R|^2$ that scales as $\sim 1 + 2\alpha$. Thus, up to first order in α, we can neglect the longitudinal term $A_L^R(\mathbf{k})$ and write $\boldsymbol{A}^R(\mathbf{k}) \simeq \hat{\mathbf{x}}_r A_p^R + \hat{\mathbf{y}} A_s^R$. Moreover, for small shifts X_λ and Y_λ one can write $1 + iX_\lambda U - iY_\lambda V \simeq \exp(iX_\lambda U - iY_\lambda V)$, and in the Cartesian coordinate system attached to the reflected beam $\chi(\tilde{\mathbf{r}},t) = \exp[i(-UX + VY + WZ)]\exp(-i\omega t)$, with $X = k_0 x_r$, $Y = k_0 y$, and $Z = k_0 z_r$, where z_r is the distance from the waist of the incident beam to the quadrant detector measured along the trajectory of the beam. Thus, Eq. (8) can be rewritten as

$$A_\lambda^R(\mathbf{k}) \simeq f_\lambda r_\lambda \chi(-X + X_\lambda, Y - Y_\lambda, Z, t). \tag{11}$$

The passage from the single plane-wave field $\boldsymbol{A}^R(\mathbf{k})$ to the total electric field $\mathbf{E}^R(\mathbf{r},t)$ is realized by substituting the plane-wave scalar amplitude $\chi(\mathbf{r},t)$ into Eq. (11), with the electric-field scalar amplitude $E(\mathbf{r},t)$ describing the spatial distribution of the incident beam. In the present case, because we want to study the behavior under reflection of OAM beams, we choose $E(\mathbf{r},t) = \psi_\ell(\mathbf{r})\exp(-i\omega t)$, $\psi_\ell(\mathbf{r})$ being the Laguerre-Gauss paraxial field with OAM index $\ell \in \{0, \pm 1, \pm 2, \ldots\}$ and radial index $p = 0$: $\psi_\ell(X,Y,Z) \propto \exp[-(X^2 + Y^2)/(2\Lambda + i2Z)]\,(X + is_\ell Y)^{|\ell|}$, with $s_\ell = \mathrm{sign}(\ell)$ and $\Lambda = k_0(k_0 w_0^2/2)$ denoting the dimensionless Rayleigh range of the beam with waist w_0 [25]. Thus, the transverse electric field of a Laguerre-Gauss beam reflected by a plane interface can be written as

$$E_\lambda^R(\mathbf{r},t) \simeq f_\lambda r_\lambda \psi_\ell(-X + X_\lambda, Y - Y_\lambda, Z)\exp(-i\omega t). \tag{12}$$

In this expression the terms X_λ and Y_λ are responsible for the GH [8] and IF [19] shifts of the center of the beam, respectively. These displacements can be assessed by measuring the position of the center of the reflected beam with a quadrant detector centered at $x_r = 0, y = 0$ along the reference axis z_r attached to the reflected central wave vector $\tilde{\mathbf{k}}_0 = k_0\hat{\mathbf{z}}_r$. A quadrant detector has four sensitive areas, denoted a, b, c, and d in the inset of Fig. 1, each delivering a photocurrent I_a, I_b, I_c, and I_d, respectively, when illuminated. The two currents $I_x = (I_a + I_b) - (I_c + I_d)$ and $I_y = (I_b + I_d) - (I_a + I_c)$ are thus proportional to the x and the y displacement of the beam intensity distribution relative to the center of the detector, respectively.

If $\ell = 0$, $\psi_0(-X + X_\lambda, Y - Y_\lambda)$ reduces to a shifted fundamental Gaussian beam, and in the hypothesis of small deviations $X_\lambda, Y_\lambda \ll 1$, a straightforward calculation furnishes

$$\frac{I_x}{I} = N_0\left(\Delta_{\mathrm{GH}} + \frac{Z}{\Lambda}\Theta_{\mathrm{GH}}\right), \quad \frac{I_y}{I} = N_0\left(\Delta_{\mathrm{IF}} + \frac{Z}{\Lambda}\Theta_{\mathrm{IF}}\right), \tag{13}$$

where $I = I_a + I_b + I_c + I_d$ and $N_0 = \sqrt{2/(\pi\sigma^2)}$, with $\sigma^2 = (\Lambda/2)\sqrt{1 + Z^2/\Lambda^2}$. Here we have defined the two spatial (Δ) and the two angular (Θ) shifts,

$$\Delta_{\mathrm{GH}} = \sum_{\lambda=p,s} w_\lambda \mathrm{Re}(X_\lambda), \quad \Delta_{\mathrm{IF}} = \sum_{\lambda=p,s} w_\lambda \mathrm{Re}(Y_\lambda), \tag{14}$$

and

$$\Theta_{\mathrm{GH}} = \sum_{\lambda=p,s} w_\lambda \mathrm{Im}(X_\lambda), \quad \Theta_{\mathrm{IF}} = \sum_{\lambda=p,s} w_\lambda \mathrm{Im}(Y_\lambda), \tag{15}$$

respectively, where the non-negative coefficients w_λ are defined as the fraction of the electric-field energy with polarization $\lambda = p,s$ in the reflected beam:

$$w_\lambda \equiv \frac{|r_\lambda f_\lambda|^2}{|r_p f_p|^2 + |r_s f_s|^2}. \tag{16}$$

If $\ell \neq 0$, Eq. (13) becomes

$$\frac{I_x}{I} = N_\ell\left(\Delta_{\mathrm{GH}}^\ell + \frac{Z}{\Lambda}\Theta_{\mathrm{GH}}^\ell\right), \quad \frac{I_y}{I} = N_\ell\left(\Delta_{\mathrm{IF}}^\ell + \frac{Z}{\Lambda}\Theta_{\mathrm{IF}}^\ell\right), \tag{17}$$

where $N_\ell = N_0\Gamma(|l|+1/2)/\left[\Gamma(|l|+1)\sqrt{\pi}\right]$ [$\Gamma(x)$ denotes the Γ function] and

$$\begin{bmatrix} \Delta^\ell_{\rm GH} \\ \Theta^\ell_{\rm IF} \\ \Delta^\ell_{\rm IF} \\ \Theta^\ell_{\rm GH} \end{bmatrix} = \begin{bmatrix} 1 & -2\ell & 0 & 0 \\ 0 & 1+|2\ell| & 0 & 0 \\ 0 & 0 & 1 & 2\ell \\ 0 & 0 & 0 & 1+|2\ell| \end{bmatrix} \begin{bmatrix} \Delta_{\rm GH} \\ \Theta_{\rm IF} \\ \Delta_{\rm IF} \\ \Theta_{\rm GH} \end{bmatrix}. \quad (18)$$

Equation (18) clearly displays the mixing between spatial and angular GH and IF shift, occurring only for $\ell \neq 0$, and it is in agreement with the results presented in Ref. [19], apart from the factor "2" in front of ℓ [26]. Notice that the polarization dependence of the four ℓ-dependent shifts on the left side of Eq. (18) resides in the four ℓ-independent shifts on the right side of the same equation. It turns out that the 4×4 mixing matrix itself is polarization independent. It should be noticed that in TIR, in contrast to partial reflection, both GH and IF angular shifts $\Theta_{\rm GH}$ and $\Theta_{\rm IF}$ are identically zero since the Fresnel coefficients are purely imaginary [27]. Thus, in this case it follows from Eq. (18) that mixing vanishes.

III. EXPERIMENTAL SETUP

Our experimental setup is shown in Fig. 2. A home-built HeNe laser ($\lambda_0 = 633$ nm) is forced to operate in a single higher-order Hermite-Gaussian (HG_{nm}) mode with $m = 0$ by insertion of a 40-μm-diameter wire normal to the axis of the laser cavity [28]. The HG_{n0} beam is sent through an astigmatic mode converter consisting of two cylinder lenses, with their common axis oriented at 45° relative to the intracavity wire. This introduces a Gouy phase which converts the HG_{n0} beam to a $LG_{\ell p}$ beam with $\ell = n$ and $p = 0$ [28]. Lenses 1 and 2 are used for mode matching; the beam leaving lens 2 is collimated with a waist parameter $w_0 = 775$ μm, a power of typically 600 μW, and a polarization set by a linear polarizer. We have incorporated the option to greatly enhance the angular spread of the beam by inserting lens 3 ($f = 70$ mm), leading to $w_0 = 19$ μm. Either with or without lens 3 present, the beam is externally reflected by the base plane of a glass prism (BK7, $n = 1.51$). We measured the polarization-differential shifts of the reflected $LG_{\ell 0}$ beam with a calibrated quadrant detector. We also obtained these shifts for the fundamental LG_{00} beam

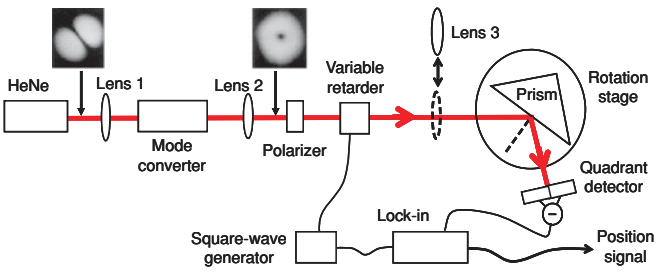

FIG. 2. (Color online) Experimental setup. The insets show the HG_{10} and LG_{10} mode profiles. The quadrant detector measures the OAM-controlled shift of the reflected beam in the plane of incidence (GH shift) and perpendicular to it (IF shift). Both the GH shift and the IF shift have a spatial and an angular contribution. See text for further details.

(=TEM_{00}) by simply removing the intracavity wire from the HeNe laser.

It follows from Eqs. (13)–(17) that using a collimated incident beam, that is, $\Lambda \gg Z$, leads to total predominance of the spatial shift. On the other hand, the use of a focused beam, that is, $\Lambda \ll Z$, leads to total predominance of the angular shift. These two extreme cases were realized in our experiment by the removal (respectively, insertion) of lens 3. Specifically, the value of the Rayleigh range $L = k_0 w_0^2/2$ was 2.96 m and 1.8 mm, respectively; as standard we have chosen the distance z_r between the beam waist and the quadrant detector to be 9.5 cm. We experimentally checked the angular nature of the shift (where expected) by verifying that the detector signal depended linearly on changes in z_r.

We performed all measurements by periodically (2.5 Hz) switching the polarization of the incident beam with a liquid-crystal variable retarder and synchronously measuring (with a lock-in amplifier) the relative beam position for one polarization with respect to the other [5,29]. Experimentally, we were restricted to using the first-order LG modes ($\ell = \pm1$) by the low gain of the HeNe laser.

IV. EXPERIMENTAL RESULTS AND COMPARISON WITH THEORY

Our experimental results for the polarization-differential shifts versus the angle of incidence are reported in Fig. 3, together with the theoretical curves ($\ell = 0$ and $\ell = \pm1$) which are based upon Eqs. (13)–(17). The four panels show the spatial and angular varieties of GH and IF shifts. Note that we have plotted here the true GH and IF shifts Δ/k_0 and

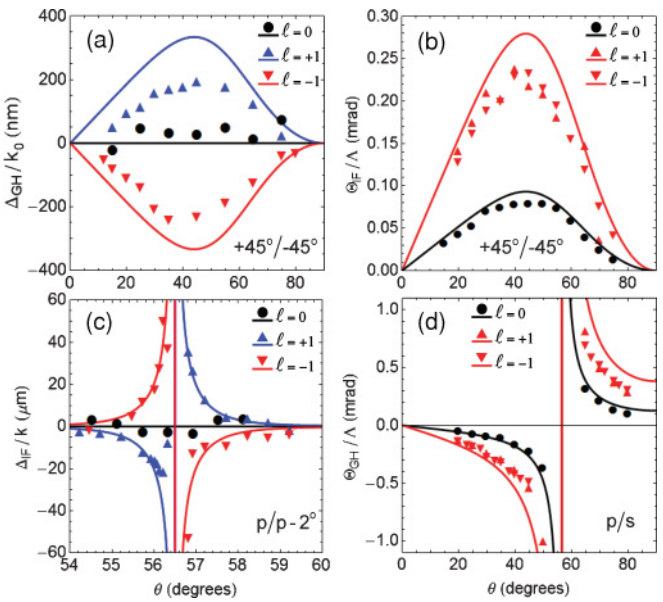

FIG. 3. (Color online) Reflective beam shift for partial dielectric reflection from an air-glass interface as a function of the angle of incidence. Plotted curves are the theoretical polarization-differential shifts for the two polarizations indicated in each panel. Experimental data and theoretical curves refer to $\ell = 0$ and $\ell = \pm1$. The panels display the spatial GH shift (a), angular IF shift (b), spatial IF shift (c), and angular GH shift (d). Here $k_0 = 2\pi/\lambda_0$; see text for further details.

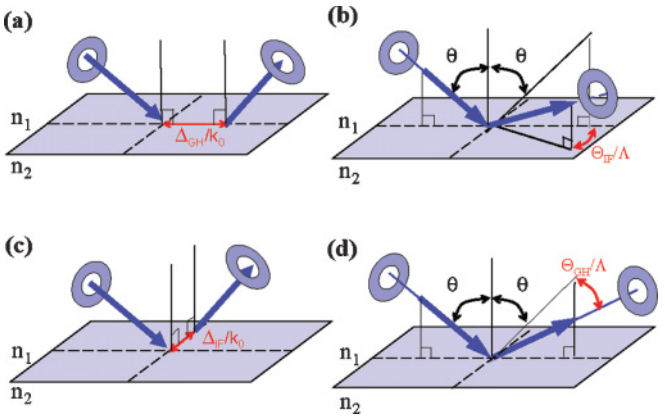

FIG. 4. (Color online) Reflection of an OAM-carrying Laguerre-Gaussian (LG) beam at a dielectric interface. Depending on the input polarization, this may lead to a longitudinal shift (GH effect) or to a transverse shift (IF effect), where longitudinal and transverse refer to the plane of incidence. Each of these shifts consists of a spatial part and an angular part, which are observed, respectively, in the near field and in the far field of the LG beam. The magnitude of the shifts increases with the OAM index ℓ. (a) The spatial GH effect; (b) the angular IF effect; (c) the spatial IF effect; (d) the angular GH effect. Note that Δ and Θ are dimensionless quantities; Λ and k_0 are the dimensionless Rayleigh range and the wave number of the LG beam, respectively. See text for further details.

Θ/Λ, respectively, and not the dimensionless shifts Δ and Θ. In each individual case the polarization modulation basis has been chosen so as to maximize the magnitude of the OAM effect.

Figure 4 shows a cartoonlike representation of the four cases that we address.

The overall agreement between experiment and theory is reasonable if we realize that there is no fitting parameter involved; we ascribe the remaining discrepancies to insufficient modal purity of the LG_{10} beam (we are very sensitive to this since we use a quadrant detector).

Figure 3(a) shows the spatial GH shift for a polarization basis of diagonal linear polarizations. In this case, the GH shift is absent for $\ell = 0$ but it appears for $\ell = \pm 1$; the sign of the shift reverses when going from $\ell = +1$ to $\ell = -1$. In Fig. 3(b) we show that the angular IF shift is different for $\ell = 0$ and $\ell = \pm 1$, using again diagonal linear polarizations. No difference occurs for $\ell = +1$ versus $\ell = -1$. Proceeding to Fig. 3(d) we observe an angular GH shift when using a linear polarization basis (s, p) for both $\ell = 0$ and $\ell = \pm 1$. Both cases show a dispersive resonance at the Brewster angle; for $\ell = 0$ these experimental results have been reported recently [5], whereas the data for $\ell = \pm 1$ (with opposite sign for $\ell = +1$ and $\ell = -1$) are new. Figure 3(c) shows the OAM dependence of the spatial IF shift, observed in a linear polarization basis $(p, p - 2^\circ)$ [21,30]. Here the shift is zero for $\ell = 0$, whereas it shows a dispersive Brewster resonance for $\ell = \pm 1$ (with opposite sign for $\ell = +1$ and $\ell = -1$).

Finally, we have confirmed experimentally that OAM did not affect spatial and angular GH and IF shifts in the TIR case (not shown); TIR was realized by flipping the glass prism in Fig. 2.

V. CONCLUSIONS

We have presented a unified theoretical description of how the OAM of a light beam affects its kinematic degrees of freedom when the beam is reflected by a dielectric interface. Without OAM the reflection leads to four beam shifts relative to geometrical optics, namely, the GH and IF shifts, each of which may have a positional and an angular part. We introduce a 4×4 polarization-independent (but ℓ-dependent) coupling matrix that describes the OAM-induced mixing of these four shifts when using a quadrant detector. Experimentally, we have confirmed this theory by measuring the four shifts as a function of the angle of incidence, for OAM values $\ell = 0$ and ± 1. We have observed for the first time the OAM-induced spatial GH shift as well as the OAM-affected angular GH and IF shifts [see Figs. 3(a)–3(c)]. Extension of all this from reflection to transmission (i.e., refraction) is straightforward.

Understanding these effects is important since they generally affect control of OAM beams by mirrors and lenses. The angular shifts are particularly interesting from a metrology point of view, both classically and quantum mechanically, since the corresponding transverse excursion of the beam center grows without limits when the beam propagates; this greatly promotes its detectability [5,31].

ACKNOWLEDGMENTS

We thank K. Y. Bliokh for stimulating us to measure the OAM-induced GH shift which acted as the seed of this article. Our work is part of the program of the Foundation for Fundamental Research of Matter (FOM). It is also supported by the European Union within FET Open-FP7 ICT as part of the STREP Program 255914 PHORBITECH. A.A. acknowledges support from the Alexander von Humboldt Foundation.

[1] I. Newton, *Opticks* (reprinted by Dover, New York, 1952); see Query 4 on p. 339.
[2] F. Goos and H. Hänchen, Ann. Phys. (Leipzig) **436**, 333 (1947).
[3] C. Imbert, Phys. Rev. D **5**, 787 (1972).
[4] F. I. Fedorov, Dokl. Akad. Nauk SSSR **105**, 465 (1955).
[5] M. Merano, A. Aiello, M. P. van Exter, and J. P. Woerdman, Nat. Photonics **3**, 337 (2009).
[6] O. Hosten and P. Kwiat, Science **319**, 787 (2008).
[7] K. Y. Bliokh, A. Niv, V. Kleiner, and E. Hasman, Nat. Photonics **2**, 748 (2008).
[8] A. Aiello and J. P. Woerdman, Opt. Lett. **33**, 1437 (2008).
[9] K. Artmann, Ann. Phys. (Leipzig) **2**, 87 (1948).
[10] K. Y. Bliokh and Y. P. Bliokh, Phys. Rev. Lett. **96**, 073903 (2006).
[11] K. Y. Bliokh and Y. P. Bliokh, Phys. Rev. E **75**, 066609 (2007).

[12] D. Felbacq, A. Moreau, and R. Smaali, Opt. Lett. **28**, 1633 (2003).
[13] V-O. de Haan, J. Plomp, T. M. Rekveldt, W. H. Kraan, A. A. van Well, R. M. Dalgliesh, and S. Langridge, Phys. Rev. Lett. **104**, 010401 (2010).
[14] A. Mair, A. Vaziri, G. Weihs, and A. Zeilinger, Nature (London) **412**, 313 (2001).
[15] H. He, M. E. J. Friese, N. R. Heckenberg, and H. Rubinsztein-Dunlop, Phys. Rev. Lett. **75**, 826 (1995).
[16] V. G. Fedoseyev, Opt. Commun. **193**, 9 (2001).
[17] V. G. Fedoseyev, J. Phys. A **41**, 505202 (2008).
[18] V. Fedoseyev, Opt. Commun. **282**, 1247 (2009).
[19] K. Y. Bliokh, I. V. Shadrivov, and Y. S. Kivshar, Opt. Lett. **34**, 389 (2009).
[20] H. Okuda and H. Sasada, J. Opt. Soc. A **25**, 881 (2008).
[21] R. Dasgupta and P. K. Gupta, Opt. Commun. **257**, 91 (2006).
[22] Y. Fainman and J. Shamir, Appl. Opt. **23**, 3188 (1984).
[23] A. Aiello, C. Marquardt, and G. Leuchs, Opt. Lett. **34**, 3160 (2009).
[24] R. F. Gragg, Am. J. Phys. **56**, 1092 (1988).
[25] L. Mandel and E. Wolf, *Optical Coherence and Quantum Optics*, 1st ed. (Cambridge University Press, Cambridge, UK, 1995).
[26] Here we quantify the GH and IF shifts via the photocurrents I_x/I and I_y/I delivered by the quadrant detector actually used in the experiment, respectively. This furnishes the *median* of the beam intensity distribution. Conversely, in Ref. [19] the same displacements are quantified via the *mean* of the intensity distribution. The difference between these two methods leads to both the trivial prefactor N_ℓ (experimentally eliminated by a detector calibration procedure) and the terms "2ℓ" (instead of "ℓ") in the mixing matrix (18).
[27] A. Aiello, M. Merano, and J. P. Woerdman, Phys. Rev. A **80**, 061801(R) (2009).
[28] M. W. Beijersbergen, L. Allen, H. E. L. O. van der Veen, and J. P. Woerdman, Opt. Commun. **96**, 123 (1993).
[29] M. Merano, A. Aiello, G. W. 't Hooft, M. P. van Exter, E. R. Eliel, and J. P. Woerdman, Opt. Express **15**, 15928 (2007).
[30] In this case maximum modulation of the beam shift is achieved by switching the (linear) polarization beween p and s. However, instead of this we have chosen to switch the polarization between p and $p - 2^\circ$. This was done to reduce the very large intensity contrast occurring during $p \leftrightarrow s$ modulation and thus to minimize a parasitic cross-effect on the displacement as synchronously measured by the quadrant detector.
[31] N. Treps, N. Grosse, W. P. Bowen, C. Fabre, H.-A. Bachor, and P. K. Lam, Science **301**, 940 (2003).

Published in Proc. of SPIE Vol. 7950, 79500F, pp 1-7, doi.101117/12.876253

Orbital angular momentum induced beam shifts

N. Hermosa*[a], M. Merano[a], A. Aiello[b], J.P. Woerdman[a]
[a]Huygens Laboratory, Leiden University, P.O. Box 9504, 2300 RA Leiden, The Netherlands;
[b]Max Planck Institute for the Science of Light, Günther-Scharowsky-Straβe 1/Bau 34, 91058 Erlangen, Germany

Abstract

We present experiments on Orbital Angular Momentum (OAM) induced beam shifts in optical reflection. Specifically, we observe the spatial Goos-Hänchen shift in which the beam is displaced parallel to the plane of incidence and angular Imbert-Fedorov shift which is a transverse angular deviation from geometric optics prediction. Experimental results agree well with our theoretical predictions. Both beam shifts increase with the OAM of the beam; we have measured these for OAM indices up to 3. Moreover, the OAM couples these two shifts. Our results are significant for optical metrology since optical beams with OAM have been extensively used in both fundamental and applied research.

Keywords: Orbital angular momentum (OAM), Goos-Hänchen shift, Imbert-Fedorov shift

1. INTRODUCTION

It is well established that a bounded beam upon reflection and transmission on a planar interface differs in propagation with plane waves due to diffraction corrections. The more dominant shifts are the Goos-Hänchen[1] (GH) shift in which the beam is displaced parallel to the plane of incidence, and the Imbert-Federov[2] (IF) shift in which the shift is perpendicular. Moreover, it has been shown that each of these two beam shifts can be separated into a spatial and an angular shift.[3] The main distinction between spatial and angular shifts is the enhancement of the latter with the propagation of the beam.

Angular Goos-Hänchen (AGH) shifts and angular Imbert-Fedorov (AIF) shifts occur only in the case of partial reflection.[3] Fig.1 shows a schematic representation of these shifts. The centroid of the reflected beam is deflected with a small angular deviation with respect to the geometric optics center. These small deviations, described by Aiello and Woerdman[3] as AGH and AIF shifts (as opposed to the conventional spatial shifts), can drastically affect the measured shifts in the position of the beam under certain experimental conditions, such as when the beam is focused. In this case, the centroid of the beam's excursion increases as the beam propagates. Merano et al.[4] showed experimental proof of the AGH effect while a quantum version of the AIF effect - the spin Hall effect of light - was demonstrated by Hosten and Kwiat[5].

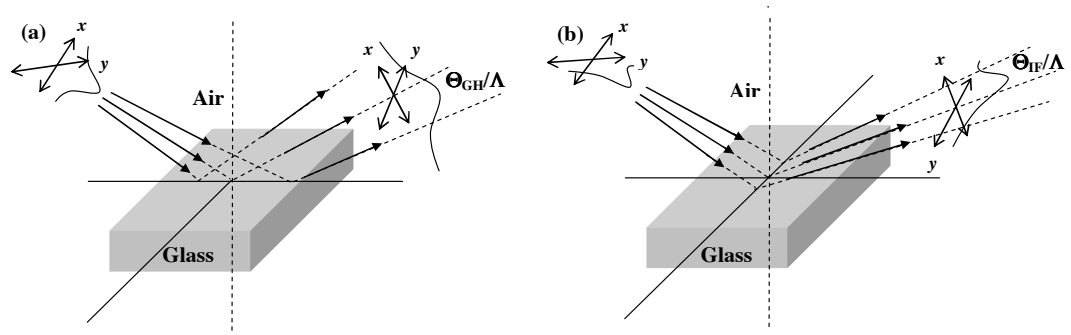

Figure 1: Schematic of the (a) Angular Goos-Hänchen and (b) Angular Imbert-Federov shifts when a beam reflects from air to glass. Θ_{GH}/Λ and Θ_{IF}/Λ are the deflection with respect to the geometric optics center (in radians), $\Lambda = kL$ where k is the wave number and L is the Rayleigh length of the beam.

*hermosa@molphys.leidenuniv.nl; Huygens Laboratory

Recently, the GH and IF shifts were extended theoretically for the case of beams with Orbital Angular Momentum (OAM).[6,7] Fedoseyev[6] calculated spatial and angular IF shifts that depended on the beam's OAM. Bliokh[7], on the other hand, described the OAM-induced coupling between angular and spatial GH and IF shifts. Experimentally, Dasgupta and Gupta[8] verified the OAM-induced IF shift predicted by Fedoseyev but only for the spatial case.

We presented the complete four OAM-induced beam shifts- spatial GH and IF, and there angular cases, for $\ell = 1, -1$ in our recent publication.[9] In the present paper, we report for the first time experimental measurements of the OAM-induced spatial GH shift angular and IF shift for a beam with higher ℓ. We show that these shifts are coupled by the OAM and increased proportionally to ℓ. We compare this to our theoretical predictions derived directly from Snell's law and Fresnel equations. Also, we verify the angular nature of the IF shift by measuring the deflection of the beam as we move the detection distance.

1.1 Theory

The electric field of an LG beam for the case of p = 0 is given by,

$$u_{\ell 0}^{LG}(r,\varphi,z) \propto \exp\left(i\frac{k}{2}\frac{r^2}{z-iL}\right) r^{\ell} \exp(i\ell\varphi) \tag{1}$$

where r, φ, z are the coordinates, ℓ is the azimuthal mode index, k is the wave number, $L = \frac{1}{2}k\omega_0^2$ is the Rayleigh range, and ω_0 is the beam waist. The reflected electric field is calculated based on the fact that the reflecting surface acts upon each plane wave in the incident field with different Fresnel coefficients. This results in a complex shift, with an imaginary part corresponding to an angular shift ("tilt"), and a real part corresponding to a spatial shift.[3] The resulting lateral and transverse displacements of the beam are combinations of both angular and spatial contributions given by;

$$\langle X \rangle(z,\ell) = \frac{1}{k}\left[\Delta_{GH}(\ell=0) - 2\ell\Theta_{IF}(\ell=0) + \frac{z}{L}\left(1+2|\ell|\right)\Theta_{GH}(\ell=0)\right] \tag{2}$$

$$\langle Y \rangle(z,\ell) = \frac{1}{k}\left[\Delta_{IF}(\ell=0) - 2\ell\Theta_{GH}(\ell=0) + \frac{z}{L}\left(1+2|\ell|\right)\Theta_{IF}(\ell=0)\right] \tag{3}$$

where $\frac{\Delta_{IF}(\ell=0)}{k}$ and $\frac{\Delta_{GH}(\ell=0)}{k}$ are the transverse and lateral spatial shifts for a Gaussian beam, respectively, and $\frac{z}{L}\Theta_{IF}(\ell=0)$ and $\frac{z}{L}\Theta_{GH}(\ell=0)$ are the transverse and lateral angular shifts also for a Gaussian beam, respectively. For a complete derivation of these quantities, we refer you to references 3 and 9. Though the calculation method was different from the one employed by Bliokh[7], the results obtained were similar, except for the factor of '2' which is due to our use of a quadrant detector.

2. EXPERIMENT

Laguerre-Gaussian (LG) beams were used in the experimental setup shown in Fig. 2. LG beams have well-defined OAM equivalent to $\ell\hbar$ per photon.[10] To be able to produce such beams, an open cavity HeNe laser (632.8nm) was used and forced to oscillate in higher order Hermite-Gaussian modes with a 40μm-diameter wire at the axis of the beam. These beams were then converted into higher-order LG modes by two cylindrical lenses as implemented by Beijersbergen et al[10]. Lens 1 and 2 were used for mode-matching in such a way that the beam left lens 2 collimated. Lens 3 focused the beam into a waist of $\omega_0 = 19\mu m$ to enhance its angular spread. The beam was reflected by a prism glass (BK7, n = 1.51) supported by a stage whose rotation angle can be controlled. The beam's excursion in the transverse and lateral positions was detected by a calibrated quadrant detector (New Focus 2901) when the input polarization was periodically varied between 45^0 and -45^0 with a liquid crystal variable retarder. A lock-in amplifier was used to reduce technical noise.

We measure the angular nature of the shift in a separate experiment using the same setup. Here, the angle of incidence was held constant while the distance of the quadrant detector to the position of the focus was varied.

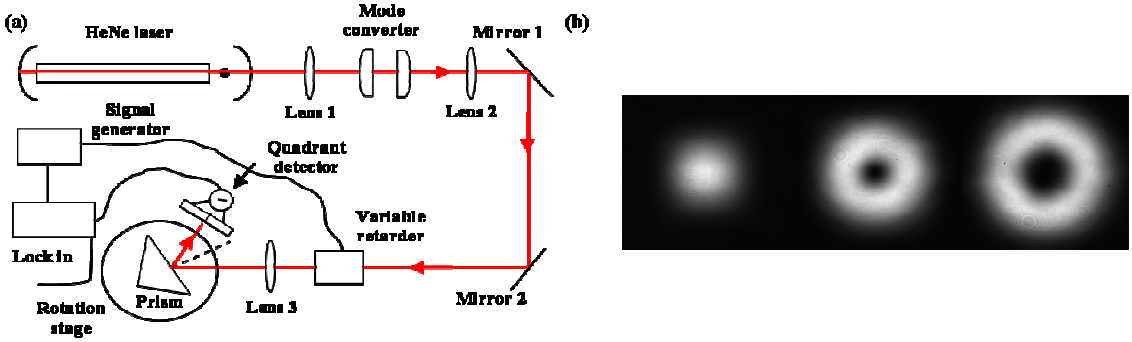

Figure 2. (a) The experimental setup. (b) LG beams produced before passing through Lens 3 (left to right, LG_{00}, LG_{01}, LG_{02})

3. RESULTS AND DISCUSSION

We measured the beam shifts with linearly polarized beams where we switched the polarization between 45^0 and -45^0; and under external reflection. Hence, eqns. 2 and 3 reduce to the following expressions;

$$\langle X \rangle(z,\ell) = \frac{-2\ell\Theta_{IF}(\ell=0)}{k} \tag{4}$$

$$\langle Y \rangle(z,\ell) = \frac{z}{kL}\left(1+2|\ell|\right)\Theta_{IF}(\ell=0) \tag{5}$$

where $\Theta_{IF}(0) = \frac{\cot\theta}{R_P^2+R_S^2}\left(R_P^2-R_S^2\right)$ is the angular IF shift of a Gaussian beam, $r_A(\theta) = R_A(\theta)\exp(i\phi_A)$ is the Fresnel coefficient with $A \in \{P,S\}$, θ is the angle of incidence

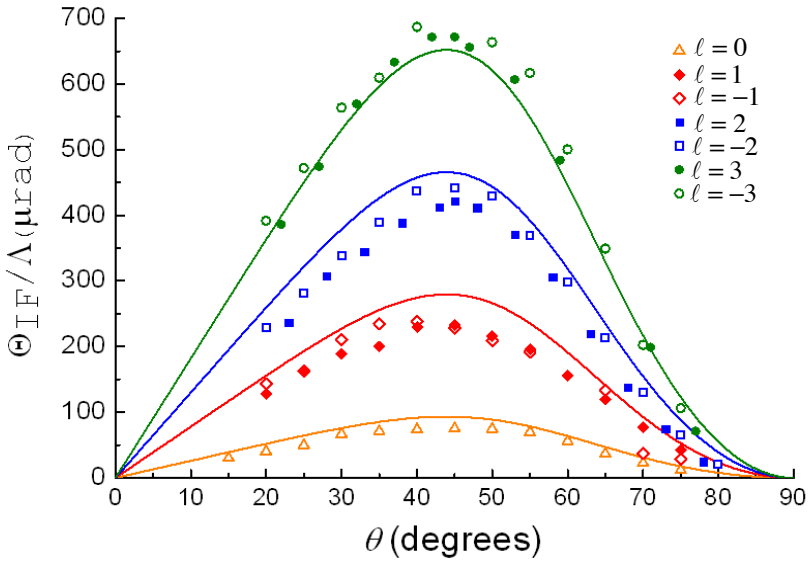

Figure 3. Angular IF shifts Θ_{IF}/Λ (radians, $\Lambda = kL$)of beams with different azimuthal mode index ℓ as a function of the angle of incidence θ . The polarization was switched between 45^0 and -45^0. The solid lines represent the theoretical curves. The filled and unfilled shapes of data points represent the positive and negative signs of ℓ , respectively. We used Δ for $\ell = 0$, ◊ for $\ell = 1$, □ for $\ell = 2$ and o for $\ell = 3$.

Figure 3 shows a plot of the polarization differential transverse shifts when the polarization of the beam is switched between 45^0 and -45^0. No fit parameter was used in the plots. The AIF or the angular tilt at small angles was determined by dividing the differential transverse shift with the distance between the quadrant detector and the waist of the beam. At any given angle of incidence, the ratios of the shifts with different ℓ's have values almost the same as the ratios of the factor $1+2|\ell|$, with the slight difference attributed to the difficulty of producing perfect higher order LG modes.

Note also that in Fig. 3 that there was no difference between the positive and negative values of ℓ in the AIF.

We verified the angular nature of the AIF by measuring the differential transverse shifts when the distance of the QD was increased. In Fig. 4, the linearly increasing value of the differential transverse spatial shifts showed the angular nature of the IF shifts. At a polarization state of 45^0, the centroid of the beam was deflected with respect to the geometric optics center. It was oppositely deflected in the case of a polarization state of -45^0. At small angles, the difference between these deflections should increase linearly, as was observed. The geometry of this has been illustrated in Fig. 5. The two linear fit lines did not cross at zero distance, as they should do theoretically. We ascribed the discrepancy to imperfections in our experimentally realized LG modes.

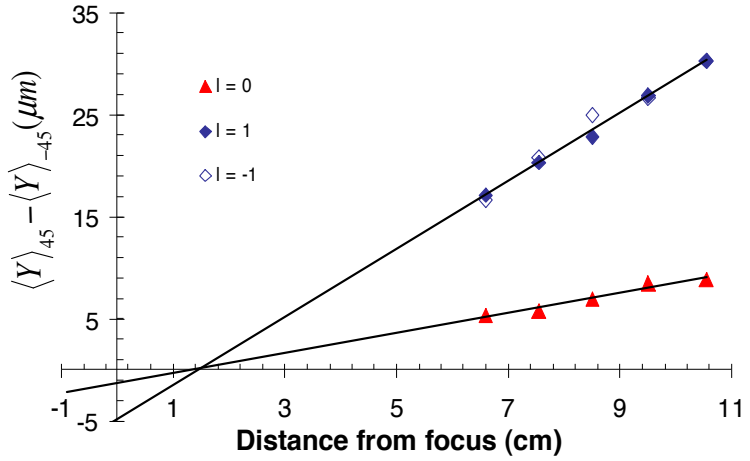

Figure 4. Transverse shifts at a constant angle of incidence θ, as the distance of the detector is changed. The lines are linear fits. As the distance of the quadrant detector is moved farther from the position of the focus, the beam's transverse excursion increases linearly proving that the shift is angular in nature.

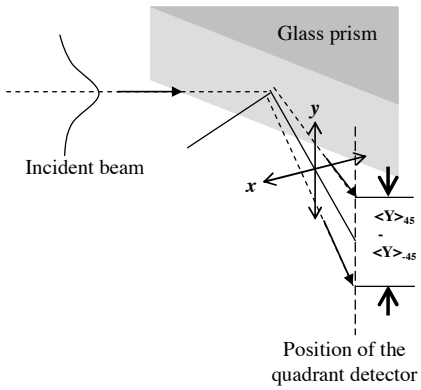

Figure 5. Transverse shifts as the distance of the detector is changed. The excursions of the beam for 45^0 and -45^0 polarization are symmetric along the axis of propagation.

The spatial Goos-Hänchen shift is zero for a planar dielectric interface for a non-OAM carrying beam in external reflection geometry. In our previous publication[9], we show experimentally that this not the case for an OAM endowed beam. Also, we verified that the maximum shift happens when the polarization is at 45^0.[9] Fig. 6 is a plot of the spatial GH shift from $\ell = -3$ to $\ell = 3$ at a constant angle of incidence of 45^0 which shows the linear dependence of the GH shift with ℓ values. The line is the theoretical fit from eqn. 4 and corresponds very well with the experimentally obtained data. A schematic diagram of the spatial GH shifts is shown in Fig. 7 as the polarization is switched.

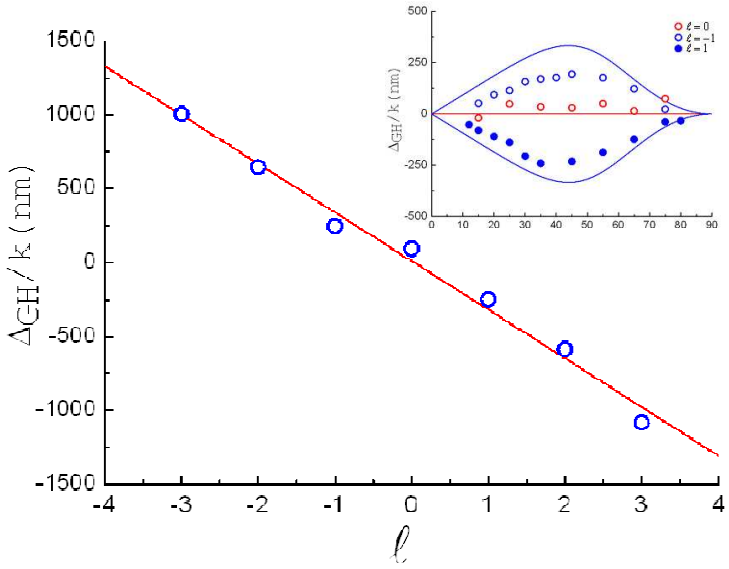

Figure 6. OAM-induced Goos-Hänchen shift at a constant angle of incidence (45^0). The shift is linear with increasing ℓ values of the beam. The inset shows the GH shift for $\ell = -1,0,1$ at different angle of incidence.

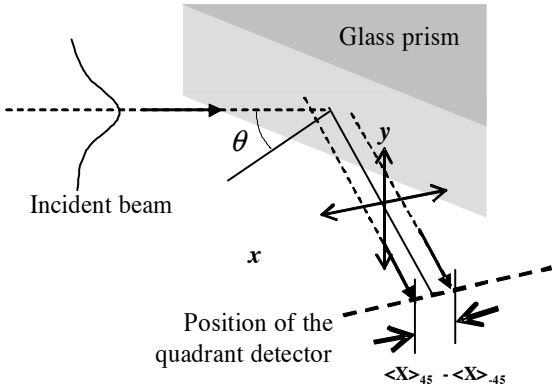

Figure 7. Schematic of the spatial GH shift. This shift on a planar dielectric in external reflection happens only for OAM carrying beams because of the coupling brought about by the OAM.

The spatial GH shift comes from the same factor responsible for the angular IF shift as seen in eqns 4 and 5. The OAM of the beam couples this factor, such that there is a spatial GH shift observed in planar dielectric surface even in external reflection. In the experiment, the AIF and the spatial GH (as shown in the inset) have the same shape except for $\ell = 0$ where the GH is zero. From experimental data on both the AIF and spatial GH shifts, we can deduce the

value of $\Theta_{IF}(\ell = 0)$ by a simple multiplication of experimental parameters, $\frac{kL}{1+2|\ell|}$ and $\frac{k}{2\ell}$ for $\ell \neq 0$, for the AIF and spatial GH, respectively. The values of $\Theta_{IF}(\ell = 0)$ from AIF and spatial GH shifts are within 5% difference with each other on average which proves the same origin of the effect.

4. CONCLUSION

We observe the spatial Goos-Hänchen (GH)shift in which the beam is displaced parallel to the plane of incidence, and the angular Imbert-Fedorov (AIF) shift which is a transverse angular deviation from geometric optics prediction. Both beam shifts are seen to increase with the OAM of the beam. Moreover, the OAM couples these two shifts. Our experimental and our theoretical predictions agree well.

The AIF shift of a beam with an OAM has been measured for $\ell = 0, 1, 2,$ and 3, when the beam reflects from a planar dielectric material. It is observed that the magnitudes of the shift increased with ℓ but are not influenced by the sign of ℓ. The angular nature of the AIF is also verified experimentally.

Moreover, the spatial GH shift is seen to be linearly dependent on ℓ and reverses its sign when the sign of ℓ is flipped. The spatial GH shift in external reflection happens only because of the OAM of the beam.

5. ACKNOWLEDGEMENTS

Our work is part of the Foundation for Fundamental Research of Matter (FOM). It is also supported by the European Union within FET Open-FP7 ICT as part of the STREP Program 255914 PHORBITECH. A.A. acknowledges support from the Alexander von Humboldt Foundation.

REFERENCES

[1] Goos, F. and Hänchen, H. ,"Ein neuer und fundamentaler versuch zur Totalreflexion," Ann. Phys. 436, 333-346 (1947).

[2] Imbert, C. , "Calculation and experimental proof of the transverse shift induced by total internal reflection of a circular polarized light beam," Phys. Rev. D 5, 787-796 (1972).

[3] Aiello, A. and Woerdman, J. P. , "Role of beam propagation in Goos-Hänchen and Imbert-Fedorov shifts," Optics Letters 33, 1437-1439 (2008).

[4] Merano, M., Aiello, A., van Exter, M. P., and Woerdman, J. P. , "Observing angular deviations in the specular reflection of a light beam," Nat. Photon. 3, 337-340 (2009).

[5] Hosten, O. and Kwiat, P. , "Observation of the Spin Hall Effect of Light via Weak Measurements," Science 319, 787-790 (2008).

[6] V. G. Fedoseyev, "Spin-independent transverse shift of the centre of gravity of a reflected or a refracted light beam," Opt. Comm. 193, 9-18 (2001).

[7] Bliokh, K. Y., Shadrivov, I. V., and Kivshar, Y. S. , "Goos-Hänchen and Imbert-Fedorov shifts of polarized vortex beams," Optics Letters 34, 389-391 (2009).

[8] Dasgupta, R. and Gupta P. K. , "Experimental observation of spin-independent transverse shift of the centre of gravity of a reflected Laguerre–Gaussian light beam," Opt. Commun 257, 91-96 (2006).

[9] Merano, M., Hermosa, N, Aiello, A., and Woerdman, J. P. , "How orbital angular momentum affects beam shifts in optical reflection," Phys. Rev. A 82, 023817 (2010).

[10] Beijersbergen, M., Allen, L, van der Veen, H. E. L. O, and Woerdman, J. P. , "Astigmatic laser mode converters and transfer of orbital angular momentum," Opt. Commun. 96, 123-132 (1993).

Spin Hall effect of light in metallic reflection

N. Hermosa,[1,*] A.M. Nugrowati,[1] A. Aiello,[2,3] and J.P. Woerdman[1]

[1] *Huygens Laboratory, Leiden University, P.O. Box 9504, 2300 RA Leiden, The Netherlands*
[2] *Max Planck Institute for the Science of Light, Günter-Scharowsky-Straße 1/Bau 24, 91058 Erlangen, Germany*
[3] *Institute for Optics, Information and Photonics, Universität Erlangen-Nürnberg, Staudtstr. 7/B2, 91058 Erlangen, Germany*
[*] *Corresponding author: hermosa@physics.leidenuniv.nl*

Compiled July 18, 2011

We report the first measurement of the Spin Hall Effect of Light (SHEL) on an air-metal interface. The SHEL is a polarization-dependent *out-of-plane* shift on the reflected beam. For the case of *metallic* reflection with a linearly polarized incident light, *both* the spatial and angular variants of the shift are observed and are maximum for $-45°/45°$ polarization, but zero for pure s- and p-polarization. For an incoming beam with circular polarization states however, only the *spatial* out-of-plane shift is present. © 2011 Optical Society of America

OCIS codes: 240.3695, 260.3910, 260.5430.

The Spin Hall Effect of Light (SHEL) is the photonic analog of the Spin Hall Effect in solid state physics in which the spin of the particles are replaced by the spin of photons (i.e. polarization) and the electric potential gradient by the refractive index gradient [1–3]. The SHEL appears as a very small but detectable polarization dependent *out-of-plane* (namely, transverse to the plane of incidence) displacement of the reflected beam at a dielectric interface relative to the geometric-optics prediction. Introduced in [1] as a transport phenomenon, the effect was in fact first theoretically derived by Fedorov in 1955 for the case of total internal reflection in glass [4]. Its experimental verification was done by Imbert in 1972 [5]; hence the SHEL is also known as the Imbert-Fedorov (IF) effect. Recently, there has been a renewed interest in the SHEL both regarding its theoretical understanding [1,2,6–8] and its potential for metrology applications. A considerable amount of experimental work has been reported for an air-dielectric interface [3, 9–13] and for an air-semiconductor interface [14].

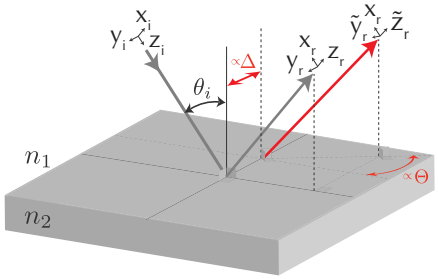

Fig. 1. (Color online) An illustration of *out-of-plane* spatial ($\propto \Delta$) and angular ($\propto \Theta$) shifts of a beam incident at an angle θ_i, upon reflection at an interface of two media.

The SHEL is part of the diffraction correction on the path of a bounded beam upon its reflection or refraction, which cannot be exactly described by the geometrical-optics (Snell's law and Fresnel formulas) alone [2]. This small correction also includes the *in-plane* shift [15], known as Goos-Hänchen (GH) shift. For both the SHEL and GH cases, there exist two variants of shift namely the spatial and angular shift; the latter being enhanced by propagation [6]. Figure 1 illustrates the spatial and angular shift for the SHEL.

In this Letter, we report for the first time, experimental measurements of the SHEL on an air-metal interface for different states of polarizations. We are interested in the SHEL on an air-metallic interface because metals have complex refractive indices, as compared to the purely real refractive indices of dielectric media.

Theoretically, a consequence of using metallic reflection has been reported previously [16], demonstrating that the spatial and angular shifts can be described by a common formalism; experimental evidence for this was provided for the GH case but not for the SHEL. Several studies have in fact shown that GH shifts is effectively a scalar effect in the sense that s- and p-polarized light undergo individual (uncoupled) GH effects [6, 17, 18]. The SHEL on the other hand, requires simultaneous s- and p-component (see Eq. 2), otherwise a transverse shift cannot occur due to symmetry reasons.

To calculate the out-of-plane shift of a beam with finite transverse extent, one can use either the law of conservation of angular momentum [1–3, 7] or more directly, using angular spectrum decomposition [6, 19]. We used the latter method to derive the equations below. The incident and reflected beams are assumed to be Gaussian; they are decomposed into plane wave components, and the Fresnel reflection coefficients are applied for both the s- and p-component of the waves, respectively. The shift is then obtained in the paraxial approximation by integrating over the reflected plane waves.

Following the notations described in Eq. (5) of [6], we express the dimensionless *out-of-plane* shift as:

$$Y_r = \Delta + Z_r \frac{\Theta}{\Lambda}, \tag{1}$$

where $Y_r = k_0 y_r$, $Z_r = k_0 z_r$, and $\Lambda = k_0(k_0 w_0^2/2) = 2/\theta_0^2$ with k_0 the wavenumber of beam center, w_0 the beam waist, and θ_0 the opening angle of the incoming beam. Eq. (1) yields the total out-of plane shift y_r that consists of two parameters with measurable units: the spatial shift Δ/k_0 as a dimensional length and the angular shift Θ/Λ in radian dimension, respectively. Variables Δ and Θ are expressed as

$$\Delta = -\frac{a_p a_s \cot\theta_i}{R_p^2 a_p^2 + R_s^2 a_s^2} \left[\left(R_p^2 + R_s^2\right)\sin\eta + 2R_p R_s \sin\left(\eta - \varphi_p + \varphi_s\right)\right], \tag{2a}$$

$$\Theta = \frac{a_p a_s \cot\theta_i}{R_p^2 a_p^2 + R_s^2 a_s^2} \left[\left(R_p^2 - R_s^2\right)\cos\eta\right], \tag{2b}$$

with $r_{s/p} = R_{s/p}\exp(i\varphi_{s/p})$ the Fresnel reflection coefficient evaluated at incident angle θ_i and $a_{s/p}$ the electric field components for perpendicular and parallel directions, respectively. The phase shift between these two components is given by η.

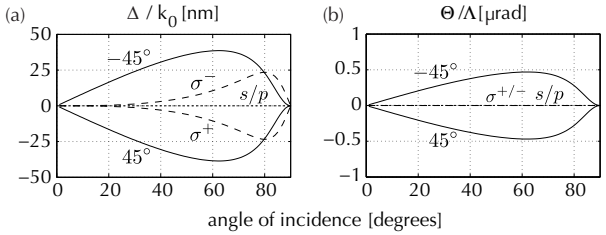

Fig. 2. Theoretical curves for (a) spatial and (b) angular shifts of linear (solid lines: $-45°/45°$, dotted lines: s/p) and circularly (dashed lines: $\sigma^{-/+}$) polarized light as a function of incident angles, calculated for gold at $\lambda = 826$ nm, $n = 1.88 + i5.39$ [20].

For a somewhat lossy surface such as gold, the difference in the phase acquired by the s- and p-component of the waves after reflection varies gradually with angle of incidence, between 0 or π [21]. The theoretical curve for various polarization states of the spatial Δ/k_0 and angular Θ/Λ shifts is shown in Fig. 2. A key distinction, as compared to the case of dielectric reflection, is that these two shifts can coexist, due to the finite losses of the metal (Au) [16]. For linearly but oblique polarized light both spatial and angular shifts contribute to the measurable beam shift y_r. The shifts are maximum at $\pm 45°$ polarization angle and becomes zero for s- and p-polarized light. Only the spatial shift occurs when using circularly polarized ($\sigma^{-/+}$) light.

Upon reflection on metal, a linearly polarized light will emerge elliptically polarized [21] due to the different phase acquired by the s- and p-component of the waves. This makes post-selection scheme necessary to observe the SHEL via a weak measurement [3, 11] impractical. We employ a different scheme, shown in Fig. 3. We use an 826 nm superluminescent light-emitting diode

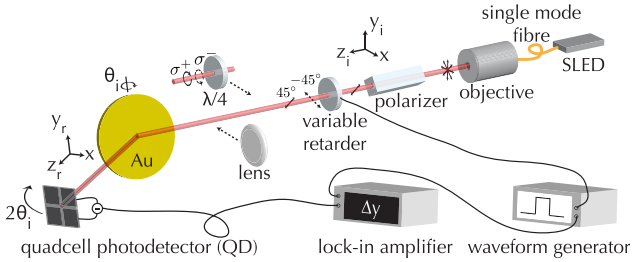

Fig. 3. (Color online) The optical set-up to measure the polarization-differential shift as a function of incident angle θ_i. See text for details.

(SLED) which is spatially filtered by a single-mode optical fiber to yield a TEM_{00} mode, collimated at a beam waist of $w_0 = 690\mu m$ and polarized by a Glan polarizer. To measure polarization-differential shifts, we switch between orthogonal polarization states ($-45°/45°$ or σ^-/σ^+) at 2.5Hz, with a liquid-crystal variable retarder (LCVR, Meadowlark). To create circularly polarized right, a QWP is inserted. Our sample is a planar (Wyko optical profiler gives 0.8 nm rms roughness) 200 nm thick Au film that is deposited on a chromium film-coated Duran ceramic glass (diameter = 10 cm, surface flateness = $\lambda/20$). The polarization-differential shifts of the reflected beam are detected by a calibrated quadcell photodetector (QD, model 2901/2921 NewFocus). To increase the opening angle of the beam, we insert a lens before the beam hits the sample. We determine the contribution of the angular shift from the measured total shift by varying the position of the detector with respect to the waist of the focused beam.

With the use of a lock-in amplifier (EG&G 5210), all measurements are performed by synchronously measuring the relative transverse position (along the y_r-axis) of the beam while switching polarizations with the LCVR. We obtained the direction (positive vs negative) of the transverse shift of the beam by noting the phase of the lock-in amplifier. Due to the different intensities between s- and p-polarization, the signal being detected by the detector and read by the lock-in amplifier needs a correction, where we have generalized the recipe in [22] for any state of polarization, into:

$$\delta y_r = \frac{\delta U}{C\Sigma_1} - \frac{U_1}{C\Sigma_1}\frac{(\Sigma_2 - \Sigma_1)}{\Sigma_1}, \tag{3}$$

with δy_r is the transverse shift in length units, δU the measured voltage difference read by the lock-in amplifier, and C the calibration constant. Note that the subscripts $\{_{1,2}\}$ are assigned to the switching polarization states in our experiments. The second term on the right hand side of Eq. (3) is the necessary correction to the read signal. It is minimum when U_1 is zero, i.e. the reflected beam with one of the switching polarization states is centered to the QD. Both U_1 and the total intensity Σ are measured by a voltmeter (HP 34401A).

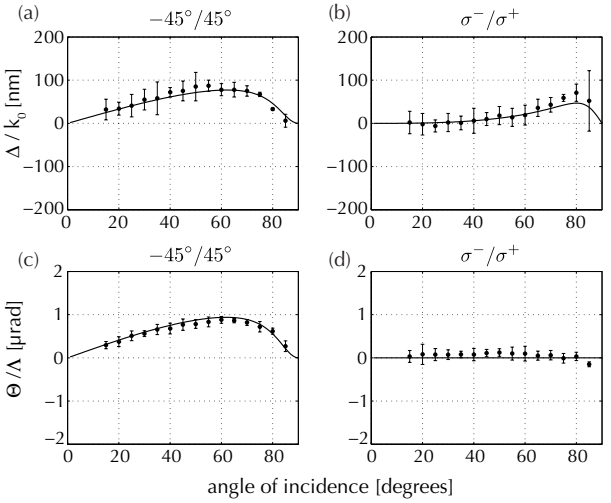

Fig. 4. Measured (top row) spatial and (bottom row) angular polarization-differential shifts between (a,c) $-45°/45°$ and (b,d) $\sigma^{-/+}$ polarized light, as a function of angle of incidence. Solid lines are theoretical curves, dots with error bars represent data with its standard deviation (3σ).

Figure 4 shows our experimental results for the polarization-differential shifts as a function of the angle of incidence together with theoretical predictions based on Eqs. (1-2). The data agrees with the theory without the use of fit parameters. The experimental error is of the order of 30 nm (to be compared with the 1 nm error in the weak-measurement method for dielectrics [3, 11]).

In Fig. 4(a) and 4(c), the angle of polarization is switched between $-45°/45°$. *Both* the out-of-plane spatial and angular polarization-differential shifts are observed and peak at an incident angle of 65°. The measurement of the spatial Fig. 4(b) and angular Fig. 4(d) polarization-differential shifts between right and left circularly polarized light ($\sigma^{-/+}$) shows that only the *spatial* out-of-plane shift is present. We have also measured the out-of-plane shift for pure *s*- and *p*-polarization (plots not shown), and the results agree with predicted zero values within the limits of uncertainty.

In agreement with theory described in Eqs. (1-2) above, our measurements of the SHEL in metal reflection do not show an existence of a backward energy flow, unlike in the GH case where the *in-plane* shift becomes negative for gold. In the GH shift, the energy flow of the evanescent field parallel to the interface changes sign when the sign of the permittivity ϵ of the reflecting medium changes [23, 24]. This argument does not hold with the SHEL in metallic reflection as the shift is perpendicular to the incoming wave vector and therefore the sign is independent of ϵ.

In summary, we have demonstrated the SHEL on an air-gold interface for different polarizations. The SHEL is specially interesting in applications where minute shift can play an important role, e.g. in metrology. On a more fundamental level, our measurements add to the understanding of how the conservation law of angular momentum plays a role when light undergoes reflection [2, 25].

This work is supported by the Foundation for Fundamental Research of Matter (FOM) and the European Union within FET Open-FP7 ICT as part of STREP Program 255914 Phorbitech.

References

1. M. Onoda, S. Murakami, and N. Nagaosa, Phys. Rev. Lett. **93**, 083901 (2004).
2. K. Y. Bliokh and Y. P. Bliokh, Phys. Rev. Lett. **96**, 073903 (2006).
3. O. Hosten and P. Kwiat, Science **319**, 787 (2008).
4. F. I. Fedorov, Dokl. Akad. Nauk SSR **105**, 465 (1955).
5. C. Imbert, Phys. Rev. D **5**, 787 (1972).
6. A. Aiello and J. P. Woerdman, Opt. Lett. **33**, 1437 (2008).
7. V. Fedoseyev, Opt. Commun. **282**, 1247 (2009).
8. H. Luo, S. Wen, W. Shu, Z. Tang, Y. Zou, and D. Fan, Phys. Rev. A **80**, 043810 (2009).
9. F. Pillon, H. Gilles, and S. Girard, Appl. Opt. **43**, 1863 (2004).
10. D. Haefner, S. Sukhov, and A. Dogariu, Phys. Rev. Lett. **102**, 123903 (2009).
11. Y. Qin, Y. Li, H. He, and Q. Gong, Opt. Lett. **34**, 2551 (2009).
12. M. Merano, N. Hermosa, J. P. Woerdman, and A. Aiello, Phys. Rev. A **82**, 023817 (2010).
13. Y. Qin, Y. Li, X. Feng, Z. Liu, H. He, Y.-F. Xiao, and Q. Gong, Opt. Express **18**, 16832 (2010).
14. J.-M. Ménard, A. E. Mattacchione, H. M. van Driel, C. Hautmann, and M. Betz, Phys. Rev. B **82**, 045303 (2010).
15. F. Goos and H. Hänchen, Annalen der Physik **436**, 333 (1947).
16. A. Aiello, M. Merano, and J. P. Woerdman, Phys. Rev. A **80**, 061801 (2009).
17. M. Merano, A. Aiello, M. van Exter, and J. Woerdman, Nat. Photon. **06** (2009).
18. M. Merano, N. Hermosa, A. Aiello, and J. P. Woerdman, Opt. Lett. **35**, 3562 (2010).
19. C.-F. Li, Phys. Rev. A **76**, 013811 (2007).
20. E. Palik, ed., *Handbook of Optical Constants of Solids* (Academic Press, New York, 1985).
21. M. Born and E. Wolf, *Principles of Optics* (Cambridge University Press, Cambridge, 1999), 7th ed.
22. M. Merano, A. Aiello, G. W. 't Hooft, M. P. van Exter, E. R. Eliel, and J. P. Woerdman, Opt. Express **15**, 15928 (2007).
23. P. Leung, C. Chen, and H.-P. Chiang, Opt. Commun. **281**, 1312 (2008).
24. H. Lai, C. Kwok, Y. Loo, and B. Xu, Phys. Rev. E **62**, 7330 (2000).
25. W. Hugrass, J. Mod. Optics **37**, 339 (1990).

Informational Fourth Page

References

1. M. Onoda, S. Murakami, and N. Nagaosa, "Hall effect of light," Phys. Rev. Lett. **93**, 083901 (2004).
2. K. Y. Bliokh and Y. P. Bliokh, "Conservation of angular momentum, transverse shift, and spin hall effect in reflection and refraction of an electromagnetic wave packet," Phys. Rev. Lett. **96**, 073903 (2006).
3. O. Hosten and P. Kwiat, "Observation of the spin hall effect of light via weak measurements," Science **319**, 787–790 (2008).
4. F. I. Fedorov, "K teorii polnogo otrazheniya," Dokl. Akad. Nauk SSR **105**, 465 (1955).
5. C. Imbert, "Calculation and experimental proof of the transverse shift induced by total internal reflection of a circularly polarized light beam," Phys. Rev. D **5**, 787–796 (1972).
6. A. Aiello and J. P. Woerdman, "Role of beam propagation in goos–hänchen and imbert–fedorov shifts," Opt. Lett. **33**, 1437–1439 (2008).
7. V. Fedoseyev, "Conservation laws and angular transverse shifts of the reflected and transmitted light beams," Opt. Commun. **282**, 1247 – 1251 (2009).
8. H. Luo, S. Wen, W. Shu, Z. Tang, Y. Zou, and D. Fan, "Spin hall effect of a light beam in left-handed materials," Phys. Rev. A **80**, 043810 (2009).
9. F. Pillon, H. Gilles, and S. Girard, "Experimental observation of the imbert-fedorov transverse displacement after a single total reflection," Appl. Opt. **43**, 1863–1869 (2004).
10. D. Haefner, S. Sukhov, and A. Dogariu, "Spin hall effect of light in spherical geometry," Phys. Rev. Lett. **102**, 123903 (2009).
11. Y. Qin, Y. Li, H. He, and Q. Gong, "Measurement of spin hall effect of reflected light," Opt. Lett. **34**, 2551–2553 (2009).
12. M. Merano, N. Hermosa, J. P. Woerdman, and A. Aiello, "How orbital angular momentum affects beam shifts in optical reflection," Phys. Rev. A **82**, 023817 (2010).
13. Y. Qin, Y. Li, X. Feng, Z. Liu, H. He, Y.-F. Xiao, and Q. Gong, "Spin hall effect of reflected light at the air-uniaxial crystal interface," Opt. Express **18**, 16832–16839 (2010).
14. J.-M. Ménard, A. E. Mattacchione, H. M. van Driel, C. Hautmann, and M. Betz, "Ultrafast optical imaging of the spin hall effect of light in semiconductors," Phys. Rev. B **82**, 045303 (2010).
15. F. Goos and H. Hänchen, "Ein neuer und fundamentaler versuch zur totalreflexion," Annalen der Physik **436**, 333–346 (1947).
16. A. Aiello, M. Merano, and J. P. Woerdman, "Duality between spatial and angular shift in optical reflection," Phys. Rev. A **80**, 061801 (2009).
17. M. Merano, A. Aiello, M. van Exter, and J. Woerdman, "Observing angular deviations in the specular reflection of a light beam," Nat. Photon. **06** (2009).
18. M. Merano, N. Hermosa, A. Aiello, and J. P. Woerdman, "Demonstration of a quasi-scalar angular goos-hänchen effect," Opt. Lett. **35**, 3562–3564 (2010).
19. C.-F. Li, "Unified theory for goos-hänchen and imbert-fedorov effects," Phys. Rev. A **76**, 013811 (2007).
20. E. Palik, ed., *Handbook of Optical Constants of Solids* (Academic Press, New York, 1985).
21. M. Born and E. Wolf, *Principles of Optics* (Cambridge University Press, Cambridge, 1999), 7th ed.
22. M. Merano, A. Aiello, G. W. 't Hooft, M. P. van Exter, E. R. Eliel, and J. P. Woerdman, "Observation of goos-hänchen shifts in metallic reflection," Opt. Express **15**, 15928–15934 (2007).
23. P. Leung, C. Chen, and H.-P. Chiang, "Addendum to "large negative goos-hänchen shift at metal surfaces", [opt. comm. 276 (2007) 206]," Opt. Commun. **281**, 1312 – 1313 (2008).
24. H. Lai, C. Kwok, Y. Loo, and B. Xu, "Energy-flux pattern in the goos-hänchen shift," Phys. Rev. E **62**, 7330 (2000).
25. W. Hugrass, "Angular momentum balance on light reflection," J. Mod. Optics **37**, 339–351 (1990).

Goos–Hänchen and Imbert–Fedorov shifts of a nondiffracting Bessel beam

Andrea Aiello[1,2,*] and J. P. Woerdman[3]

[1]*Max Planck Institute for the Science of Light, Günter-Scharowsky-Strasse 1/Bau 24, 91058 Erlangen, Germany*

[2]*Institute for Optics, Information and Photonics, University Erlangen-Nürnberg, Staudtstrasse 7/B2, 91058 Erlangen, Germany*

[3]*Huygens Laboratory, Leiden University, P.O. Box 9504, 2300 RA Leiden, The Netherlands*

**Corresponding author: andrea.aiello@mpl.mpg.de*

Received November 2, 2010; revised December 24, 2010; accepted January 20, 2011;
posted January 21, 2011 (Doc. ID 137614); published February 11, 2011

Goos–Hänchen (GH) and Imbert–Fedorov (IF) shifts are diffractive corrections to geometric optics that have been extensively studied for a Gaussian beam that is reflected or transmitted by a dielectric interface. Propagating in free space before and after reflection or transmission, such a Gaussian beam spreads due to diffraction. We address here the question of how the GH and IF shifts behave for a "nondiffracting" Bessel beam. © 2011 Optical Society of America

OCIS codes: 240.3695, 260.5430.

It has been known for a long time that the behavior of a finite-diameter light beam in reflection and transmission at a dielectric interface differs from the predictions of geometric optics. Because of diffractive corrections, the beam is shifted in directions parallel and perpendicular to the plane of incidence [1]. The parallel shift is known as the Goos–Hänchen (GH) effect [2,3], and the transverse shift is known as the Imbert–Fedorov (IF) effect [4–6]. These effects have been extensively studied not only for total internal reflection, which is the context wherein the GH and IF effects were originally addressed, but also in partial dielectric reflection and transmission [7–9]. We note that the IF effect is closely related to the spin Hall effect of light [7,10–12]. Further generalizations concern angular varieties of the GH and IF effects; these are observed in the far field of the reflected (or transmitted) beam [13]. Recently, the influence of orbital angular momentum (OAM) of the incident beam on these diffractive shifts has also been investigated [14–16]; for the transverse case, this may be called the orbital Hall effect of light [17].

The *diffractive* origin of these effects raises the question of how they behave when the incident beam is a so-called *nondiffracting* Bessel beam. Such beams were perceived by Durnin and Miceli *et al.* as propagation-invariant solutions of the free-space scalar wave equation [18,19]. These solutions have amplitudes proportional to the Bessel functions. The zero-order Bessel beam has a bright central maximum ("needle beam"), which propagates in free space without diffractional spreading; the higher-order beams have a dark central core. Most of the work on Bessel beams has been restricted to the paraxial limit [20,21], but also the nonparaxial case (described by the Helmholtz wave equation) has been reported [6,22,23].

Ideal Bessel beams have an infinite transverse diameter and cannot, therefore, be generated experimentally. However, there exist several experimental methods to generate finite-diameter approximations to a Bessel beam; these propagate over a finite axial distance in a nondiffracting manner (i.e., over distances much larger than the Rayleigh length corresponding to the needle-beam diameter) [24]. So, one may speculate that such a needle beam corresponds to a geometric optics ray that would *not* show GH and IF shifts. Verification or rebuttal of this speculation requires proper theory; this is reported in the present Letter.

Let us begin by briefly recalling what a Bessel beam is. The *scalar* mth-order Bessel beam is a cylindrically symmetric monochromatic optical beam whose electric field has the following form:

$$E(R,\varphi,z) = J_m(K_0R)e^{im\varphi}e^{iz\sqrt{k_0^2-K_0^2}} \equiv A(R,\varphi)e^{iz\sqrt{k_0^2-K_0^2}}, \tag{1}$$

where m is an integer number that fixes the value of the OAM of the beam and (R,φ,z) are the cylindrical spatial coordinates defined with respect to the main axis of propagation $\hat{\mathbf{z}}$:

$$\begin{cases} x &= R\cos\varphi, \\ y &= R\sin\varphi. \end{cases} \tag{2}$$

For a needle beam, one has $m = 0$. In Eq. (1), $k_0 > 0$ and $0 \le K_0 \le k_0$ are two *independent* parameters, where K_0 determines the *angular width* ϑ_0 of the central lobe (cone) of the corresponding Bessel function via the definition

$$K_0 = k_0 \sin\vartheta_0, \qquad (0 \le \vartheta_0 \le \pi/2). \tag{3}$$

Throughout this Letter we will consider only *paraxial* Bessel beams characterized by the condition

$$\sin\vartheta_0 = K_0/k_0 \ll 1. \tag{4}$$

It should be noticed that while $E(R,\varphi,z)$ is an exact solution to the Helmholtz equation $(\partial_x^2+\partial_y^2+\partial_z^2+k_0^2)E = 0$ in free space, the amplitude $A(R,\varphi)$ satisfies the reduced equation $(\partial_x^2+\partial_y^2+K_0^2)A = 0$.

For actual calculations of both the GH and IF shifts, it is convenient to work in Fourier space and calculate the Fourier transform $\tilde{A}(K,\phi)$ of the amplitude $A(R,\varphi) = J_m(K_0R)e^{im\varphi}$ as

$$J_m(K_0R)e^{im\varphi} = \frac{1}{2\pi}\int \tilde{A}(k_x,k_y)e^{i\boldsymbol{K}\cdot\boldsymbol{R}}\mathrm{d}k_x\mathrm{d}k_y, \qquad (5)$$

where

$$\tilde{A}(k_x,k_y) = \tilde{A}(K,\phi) = \frac{1}{i^m K_0}\delta(K-K_0)e^{im\phi}, \qquad (6)$$

with $K=(k_x^2+k_y^2)^{1/2}$, $\boldsymbol{K}\cdot\boldsymbol{R}=xk_x+yk_y=KR\cos(\phi-\varphi)$, and $k_x = K\cos\phi$, $k_y = K\sin\phi$. It is worth noticing that in the literature, Eq. (6) is often written in spherical coordinates (k_0,ϑ,ϕ) with $K=k_0\sin\vartheta$, $K_0\delta(K-K_0) = \delta(\vartheta-\vartheta_0)/\cos\vartheta_0$, and $dk_xdk_y = k_0^2\sin\vartheta\cos\vartheta d\vartheta d\phi$.

Having written explicitly the Fourier representation of a scalar Bessel beam, we can now proceed as in [17] and write the Fourier amplitude of a *vector* Bessel beam as

$$\tilde{A}(k_x,k_y) \to \tilde{\boldsymbol{A}}(k_x,k_y) = \boldsymbol{f}_\perp(\boldsymbol{K})\tilde{A}(k_x,k_y), \qquad (7)$$

where $\boldsymbol{f}_\perp(\boldsymbol{K}) = \hat{\boldsymbol{f}} - \hat{\boldsymbol{k}}(\hat{\boldsymbol{k}}\cdot\hat{\boldsymbol{f}})$, with $\hat{\boldsymbol{k}} = k_x\hat{\boldsymbol{x}} + k_y\hat{\boldsymbol{y}} + (k_0^2 - K^2)^{1/2}\hat{\boldsymbol{z}}$ and $\hat{\boldsymbol{f}} = f_p\hat{\boldsymbol{x}} + f_s\hat{\boldsymbol{y}}$, $|\hat{\boldsymbol{f}}|^2 = 1$. Here, according to [17], the three unit vectors $\{\hat{\boldsymbol{x}},\hat{\boldsymbol{y}},\hat{\boldsymbol{z}}\}$ form a right-handed Cartesian reference frame attached to the incident beam propagating along the axis $\hat{\boldsymbol{z}}$.

The spatial and angular GH and IF shifts for a Bessel beam impinging at the angle θ upon a planar interface orthogonal to $\hat{\boldsymbol{n}}$, can be calculated from Eqs. (54–62) given in Sec. III of [25] by putting $E_\lambda(k_0U,k_0V) = \hat{\boldsymbol{e}}_\lambda(\boldsymbol{k})\cdot\tilde{\boldsymbol{A}}(k_x,k_y)$, $\lambda\in\{p,s\}$, where $\hat{\boldsymbol{e}}_s(\boldsymbol{k}) = \hat{\boldsymbol{n}}\times\hat{\boldsymbol{k}}/|\hat{\boldsymbol{n}}\times\hat{\boldsymbol{k}}|$ and $\hat{\boldsymbol{e}}_p(\boldsymbol{k}) = \hat{\boldsymbol{e}}_s(\boldsymbol{k})\times\hat{\boldsymbol{k}}$, with $\hat{\boldsymbol{k}}\cdot\hat{\boldsymbol{n}} = \cos\theta$. To express the results of such a calculation, it is useful to adopt the notation introduced in [17] and to define the "intrinsic" (namely, beam-independent) longitudinal and transverse beam shifts as, respectively,

$$X_\lambda = -i\frac{\partial \ln r_\lambda}{\partial\theta} = \phi'_\lambda - i\frac{R'_\lambda}{R_\lambda}, \qquad (8)$$

$$Y_p = i\frac{f_s}{f_p}\left(1+\frac{r_s}{r_p}\right)\cot\theta, \qquad Y_s = -i\frac{f_p}{f_s}\left(1+\frac{r_p}{r_s}\right)\cot\theta, \qquad (9)$$

where $r_\lambda = R_\lambda\exp(i\phi_\lambda)$, $\lambda\in\{p,s\}$ are the Fresnel coefficient of the interface, and the prime indicates derivatives with respect to the incidence angle θ. Moreover, we rewrite the complex-valued coefficients f_p and f_s in terms of the real valued parameters a_p, a_s, and η defined as $f_p = a_p$, $f_s = a_s\exp(i\eta)$. Finally, we define the relative energies w_p and w_s of the reflected beam as

$$w_p = \frac{a_p^2R_p^2}{a_p^2R_p^2+a_s^2R_s^2}, \qquad w_s = \frac{a_s^2R_s^2}{a_p^2R_p^2+a_s^2R_s^2} \qquad (10)$$

and the complex-valued longitudinal and transversal shifts Ξ and Ψ as

$$\Xi = w_pX_p + w_sX_s, \qquad \Psi = w_pY_p + w_sY_s, \qquad (11)$$

where

$$\mathrm{Re}(\Xi) = \frac{a_p^2R_p^2\phi'_p + a_s^2R_s^2\phi'_s}{a_p^2R_p^2+a_s^2R_s^2}, \qquad (12a)$$

$$\mathrm{Im}(\Xi) = -\frac{a_p^2R_pR'_p + a_s^2R_sR'_s}{a_p^2R_p^2+a_s^2R_s^2}, \qquad (12b)$$

$$\mathrm{Re}(\Psi) = -\frac{a_pa_s\cot\theta(R_p^2+R_s^2)\sin\eta}{a_p^2R_p^2+a_s^2R_s^2} - \frac{a_pa_s\cot\theta[2R_pR_s\sin(\eta-\phi_p+\phi_s)]}{a_p^2R_p^2+a_s^2R_s^2}, \qquad (12c)$$

$$\mathrm{Im}(\Psi) = \frac{a_pa_s\cot\theta(R_p^2-R_s^2)\cos\eta}{a_p^2R_p^2+a_s^2R_s^2}. \qquad (12d)$$

At this point, we have gathered all the formulas that we need to write explicitly the results from our calculations for both GH and IF shifts of a mth-order Bessel beam. A straightforward application of Eqs. (58–59) in [25] furnishes the following results:

$$k_0\Delta_{\mathrm{GH}} \equiv k_0\langle x_r\rangle|_{z_r=0} = \mathrm{Re}(\Xi) - m\mathrm{Im}(\Psi), \qquad (13a)$$

$$k_0\Delta_{\mathrm{IF}} \equiv k_0\langle y_r\rangle|_{z_r=0} = \mathrm{Re}(\Psi) + m\mathrm{Im}(\Xi), \qquad (13b)$$

for the spatial part of the shifts and

$$\Theta_{\mathrm{GH}} \equiv \frac{\partial\langle x_r\rangle}{\partial z_r} = \sin^2(\vartheta_0)\mathrm{Im}(\Xi), \qquad (14a)$$

$$\Theta_{\mathrm{IF}} \equiv \frac{\partial\langle y_r\rangle}{\partial z_r} = \sin^2(\vartheta_0)\mathrm{Im}(\Psi), \qquad (14b)$$

for the angular part [9]. These formulas are the main result of this Letter. Here, and in the subsequent formulas, the three Cartesian coordinates $\{x_r,y_r,z_r\}$ are referred to a reference frame attached to the reflected beam of central wave vector $\tilde{\boldsymbol{k}}_0$, with z_r directed along $\tilde{\boldsymbol{k}}_0 = \boldsymbol{k}_0 - 2\hat{\boldsymbol{n}}(\hat{\boldsymbol{n}}\cdot\boldsymbol{k}_0)$ [17]. Before proceeding with the discussion of these formulas, a caveat is in order here. From Eq. (6), it follows that the electric field energy density of a Bessel beam is represented by a highly singular function (square of a Dirac-delta). However, it is possible to show that a careful treatment of such singularities (see also the discussion about angular shift [26]) always leads to finite results for the first-order moments of the electric field energy density distribution.

Some relevant issues follow from Eqs. (13) and (14) above. First, for paraxial beams where Eq. (4) holds, one has $\sin\vartheta_0\sim\vartheta_0$, and from Eqs. (14) it follows that the angular shift of a Bessel beam is a *second-order effect* in a perturbation expansion of the beam (with respect to the expansion parameter ϑ_0). This is consistent with the fact that at the first-order perturbation theory, a Bessel beam is *not* deformed upon reflection and, because its

energy density does not change during propagation, *in principle* it cannot show any angular shift [26]. In particular, for $m = 0$, i.e., for a needle beam, this fact implies that at the first order of the perturbation expansion, both GH and IF shifts also occur for the central nondiffracting core of the beam. However, this is no longer true if one goes to perturbation orders higher than two (i.e., relatively strong focusing); this reduces the length over which diffraction is effectively absent to a propagation length of the order of the diameter of the full Bessel beam.

Second, it should be noticed that for a Laguerre–Gauss beam with the same $\exp(im\phi)$ functional dependence, both GH and IF angular shifts are proportional to the "enhancement" factor $1 + |m|$ [17]. Conversely, in Eqs. (14), such a term is absent. It is not difficult to show that this is due to the term R^m, which is present in the expression of the amplitude of a Laguerre–Gauss beam but not in Eq. (1).

Finally, Eq. (13) shows a spatial/angular mixing analogous to the one present for a Laguerre–Gauss beam of OAM m first discovered in [15] and further developed in [17]. It may be shown that this mixing is a common feature of all paraxial beams with an $\exp(im\phi)$ functional dependence. However, a complete treatment for arbitrary beams in this regime is outside the scope of this Letter [27].

A. Aiello acknowledges support from the Alexander von Humboldt Foundation.

References and Notes

1. J. D. Jackson, *Classical Electrodynamics*, 3rd ed. (Wiley, 1998).
2. F. Goos and H. Hänchen, Ann. Phys. **436**, 333 (1947).
3. K. Artmann, Ann. Phys. **437**, 87 (1948).
4. F. I. Fedorov, Dokl. Akad. Nauk SSSR **105**, 465 (1955).
5. C. Imbert, Phys. Rev. D **5**, 787 (1972).
6. A. V. Novitsky and L. M. Barkovsky, J. Opt. A **10**, 075006 (2008).
7. K. Yu. Bliokh and Yu. P. Bliokh, Phys. Rev. Lett. **96**, 073903 (2006).
8. K. Yu. Bliokh and Yu. P. Bliokh, Phys. Rev. E **75**, 066609 (2007).
9. A. Aiello and J. P. Woerdman, Opt. Lett. **33**, 1437 (2008).
10. M. Onoda, S. Murakami, and N. Nagaosa, Phys. Rev. Lett. **93**, 083901 (2004).
11. O. Hosten and P. Kwiat, Science **319**, 787 (2008).
12. A. Aiello, N. Lindlein, C. Marquardt, and G. Leuchs, Phys. Rev. Lett. **103**, 100401 (2009).
13. M. Merano, A. Aiello, M. P. van Exter, and J. P. Woerdman, Nat. Photon. **3**, 337 (2009).
14. V. G. Fedoseyev, J. Phys. A **41**, 505202 (2008).
15. K. Y. Bliokh, I. V. Shadrivov, and Y. S. Kivshar, Opt. Lett. **34**, 389 (2009).
16. A. Aiello, M. Merano, and J. P. Woerdman, Opt. Lett. **34**, 1207 (2009).
17. M. Merano, N. Hermosa, J. P. Woerdman, and A. Aiello, Phys. Rev. A **82**, 023817 (2010).
18. J. E. Durnin, J. Opt. Soc. Am. A **4**, 651 (1987).
19. J. E. Durnin, J. J. Miceli, Jr., and J. H. Eberly, Phys. Rev. Lett. **58**, 1499 (1987).
20. Y. Z. Umul, J. Opt. Soc. Am. A **27**, 390 (2010).
21. G. S. McDonald, S. Chavez-Cerda, and G. H. C. New, Opt. Commun. **123**, 225 (1996).
22. M. Santarsiero, R. Borghi, and M. A. Porras, J. Opt. Soc. Am. A **18**, 1650 (2001).
23. J. Chen and Y. Yu., Opt. Commun. **283**, 1655 (2010).
24. J. Arlt and K. Dholakia, Opt. Commun. **177**, 297 (2000).
25. A. Aiello and J. P. Woerdman, "Theory of angular Goos–Hänchen shift near Brewster incidence," arXiv:0903.3730v2 (2009).
26. The point here is rather subtle. The actual reason why we can predict the existence of an angular shift is because, in our calculations, we use the rigorous definition of a Dirac-delta distribution as a kind of limit of a sequence of regular functions (specifically, Gaussian functions). Conversely, a straightforward (and formally incorrect) symbolic manipulation of products of Dirac-delta singularities would lead to the absence of such a shift.
27. A. Aiello and J. P. Woerdmanare preparing a manuscript to be called "Goos–Haenchen and Imbert–Fedorov shifts of an arbitrary paraxial beam."